JBC RESEARCH ARTICLE

Covalent conjugation of ubiquitin-like ISG15 to apoptosis-inducing factor exacerbates toxic stimuli-induced apoptotic cell death

Received for publication, December 6, 2021, and in revised form, August 27, 2022 Published, Papers in Press, September 6, 2022,
https://doi.org/10.1016/j.jbc.2022.102464

Seo Jeong Jeon and Kwang Chul Chung*

From the Department of Systems Biology, College of Life Science and Biotechnology, Yonsei University, Seoul, Korea

Edited by Alex Toker

Apoptosis-inducing factor (AIF) is a mitochondrion-localized flavoprotein with NADH oxidase activity. AIF normally acts as an oxidoreductase to catalyze the transfer of electrons between molecules, but it can also kill cells when exposed to certain stimuli. For example, intact AIF is cleaved upon exposure to DNA-damaging agents such as etoposide, and truncated AIF (tAIF) is released from the mitochondria to the cytoplasm and translocated to the nucleus where it induces apoptosis. Although the serial events during tAIF-mediated apoptosis and the transition of AIF function have been widely studied from various perspectives, their underlying regulatory mechanisms and the factors involved are not fully understood. Here, we demonstrated that tAIF is a target of the covalent conjugation of the ubiquitin-like moiety ISG15 (referred to as ISGylation), which is mediated by the ISG15 E3 ligase HERC5. In addition, ISGylation increases the stability of tAIF protein as well as its K6-linked polyubiquitination. Moreover, we found that ISGylation increases the nuclear translocation of tAIF upon cytotoxic etoposide treatment, subsequently causing apoptotic cell death in human lung A549 carcinoma cells. Collectively, these results suggest that HERC5-mediated ISG15 conjugation is a key factor in the positive regulation of tAIF-mediated apoptosis, highlighting a novel role of posttranslational ISG15 modification as a switch that allows cells to live or die under the stress that triggers tAIF release.

Apoptosis-inducing factor (AIF) and its strongly conserved homologs are ubiquitous in organisms from bacteria to vertebrates (1). AIF is synthesized in the cytosol and imported into the mitochondrial intermembrane space. AIF normally serves as a mitochondrial oxidoreductase under healthy physiological condition (2). However, a distinct proapoptotic function of AIF is displayed under stimulation with certain toxic stimuli, which is critical for cell death. For example, upon oxidative stress or depolarization of the mitochondrial membrane, membrane-bound mature AIF is cleaved through proteolytic processing into soluble AIF. The Ca^{2+}-dependent cysteine protease μ-calpain mainly cleaves AIF, and truncated AIF (tAIF) is then released into the cytoplasm (3–6). Finally, cytosolic AIF translocates to the nucleus where it primarily governs apoptosis, causing large-scale DNA breakage, chromatin condensation, and cell shrinkage, and eventually cellular apoptosis (7).

Posttranslational modification (PTM) regulates various functions of proteins and their physiological states. Similar to many other proteins, AIF could be a target of diverse PTMs. For example, PAK5 directly phosphorylates AIF at T281, suppressing its nuclear translocation and promoting the tumorigenesis of breast cancer (8). In addition, N-methyl-N-nitro-N′-nitrosoguanidine (MNNG), a genotoxic agent, induces caspase-independent but tAIF-induced apoptosis (9). Interestingly, truncated AIF released into the cytoplasm by MNNG is ubiquitinated by the ubiquitin E3 ligase CHIP, inhibiting cell death (10). CHIP also mediates the K48-linked and/or K63-linked polyubiquitination of tAIF, resulting in the proteasomal degradation of tAIF. By contrast, the ubiquitin protease USP2 catalyzes the deubiquitination of tAIF, antagonizing the CHIP-induced degradation of tAIF, thereby maintaining the stability of tAIF and finally activating apoptosis (10). AIF could also be a target of nondegradative ubiquitination at the K255 residue by X-linked inhibitor of apoptosis (XIAP), which attenuates the apoptosis-inducing activity of AIF (11, 12). Overall, these results suggest that diverse PTMs allow cells to orchestrate the structure and localization of AIF, resulting in a delicate balance of its functions, thereby modulating cell fate depending on the cell context.

Although ubiquitin is the best studied posttranslational modifier, there is a growing family of ubiquitin-like (UBL) proteins that have been reported to modify cellular targets in pathways that are parallel to, but distinct from, the ubiquitin pathway. These proteins include SUMO, NEDD8, interferon (IFN)-stimulated gene 15 (ISG15), and FAT10, and conjugation to these modifiers affects the target protein's activity and/or physiological functions. Among these, ISG15 is strongly induced in response to type I IFN (13). ISG15 is also highly induced by various toxic stimuli such as viral infection, lipopolysaccharide, and genotoxic stresses. Similar to ubiquitin, ISG15 uses the C-terminal Gly-Gly motif for conjugation to specific lysine residue of target proteins (14). In the process of

* For correspondence: Kwang Chul Chung, kchung@yonsei.ac.kr.

covalent ISG15 conjugation (referring to as ISGylation), the cooperation of E1, E2, and E3 enzymes is required, similar to ubiquitination (15). However, in contrast to the numerous ubiquitin E3 ligases that have been identified to date, only three are currently known for ISG15 E3 ligase: EFP, HHARI, and HERC5 (16). Similar to ubiquitin, ISGylation is a reversible enzymatic process, and ISG15 is removed from proteins by the deconjugating enzyme USP18 (also known as UBP43) (17). The expression of the enzymes involved in ISGylation, including UBP43, is also upregulated by IFN treatment (18).

ISGylation affects the function and physiological state of target proteins depending on the species, tissues, cell types, and external stimuli, consequently regulating various signal transduction pathways, protein ubiquitination, and the antiviral response. In addition, free ISG15 has been shown to act as a cytokine and tumor suppressor or conversely, as an oncogenic factor (19–23). Although several proteomics studies have screened for viral substrates as well as hundreds of cellular substrates of ISG15 modification (24–26), many of their regulatory mechanisms and functional consequences have yet to be elucidated in detail.

Many studies have reported that ubiquitination targets could also be conjugated by multiple UBL modifiers, including ISG15. Moreover, several studies have demonstrated that ISGylation affects target proteins and controls the balance between cell death and survival. For instance, parkin ISGylation promotes ubiquitin E3 ligase activity by inhibiting intramolecular interactions, thereby increasing the cytoprotective effect (27). ISGylation of CHIP also promotes E3 ubiquitin ligase activity and reduces oncogenic c-*myc* levels, resulting in the inhibition of tumor growth in lung carcinoma A549 cells (28).

Based on these findings, we investigated whether AIF is a novel target for ISG15 conjugation, and if that is the case, how the ISGylation affects the nuclear translocation of tAIF. Our results showed that tAIF was covalently modified by ISG15 when A549 cells were treated with etoposide, which was mediated by the HERC5 ISG15 E3 ligase. In addition, ISGylation enhanced the degradation-independent polyubiquitination of tAIF and its nuclear transport, stimulating apoptotic cell death in response to cytotoxic etoposide.

Results

Truncated AIF is a target of ISGylation in mammalian cells

To determine whether AIF is a target of ISGylation in mammalian cells, we first performed Ni-NTA pull-down assays. Human embryonic kidney 293 (HEK293) cells were cotransfected with multiple components of the ISG15-conjugating system, including UBE1L (E1), UbcH8 (E2), and FLAG-tagged ISG15 alone or with V5-His-tagged full-length AIF or its truncated mutant lacking the N-terminal domain. After cells were lysed with lysis buffer containing 8 M urea, immunoblot analyses of the samples revealed that both full-length AIF and tAIF were covalently modified by ISG15 under denaturing conditions (Fig. 1*A*). Interestingly, a single

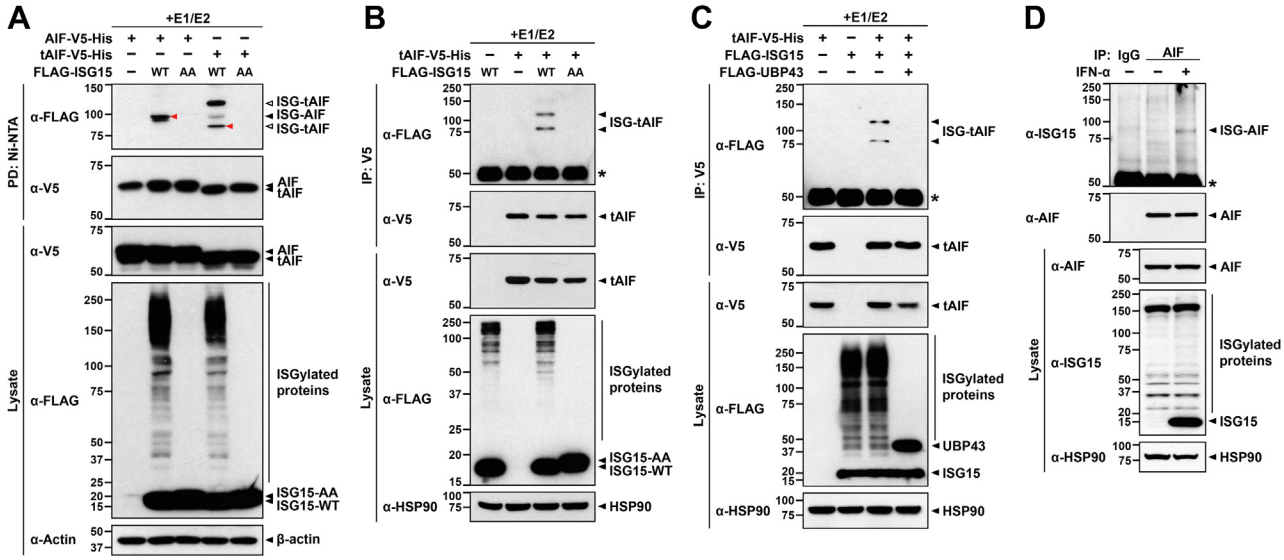

Figure 1. tAIF is a target of ISGylation. *A*, HEK293 cells were transfected for 24 h with plasmids encoding C-terminal V5-His-tagged full length AIF (AIF-V5-His) or its truncated mutant lacking the N-terminal 101 amino acids (tAIF-V5-His), FLAG-ISG15-WT, or its conjugation-defective mutant (FLAG-ISG15-AA) alone or in combination. Cell lysates were subjected to Ni-NTA pull down (PD: Ni-NTA) under denaturing conditions, followed by Western blotting with anti-FLAG or anti-V5 antibody. Closed and open arrowhead indicate the bands of ISGylated full-length AIF and tAIF, respectively. The bands marked with a *red* arrowhead on the gel were assumed to be the major ISG15-conjugated products. *B*, HEK293 cells were transfected for 24 h with plasmids encoding tAIF-V5-His, FLAG-ISG15-WT, or FLAG-ISG-AA alone or in combination. Cell lysates were immunoprecipitated using an anti-V5 antibody, followed by immunoblotting with the indicated antibodies. *C*, HEK293 cells were transfected for 24 h with plasmids encoding tAIF-V5-His, FLAG-ISG15-WT, or FLAG-UBP43 alone or in combination. Cell lysates were immunoprecipitated using an anti-V5 antibody, followed by immunoblotting with the indicated antibodies. All samples were transfected with plasmids encoding the ISG15-activating enzyme UBE1L (E1) and Myc-labeled ISG15-conjugating enzyme UbcH8 (E2). *D*, A549 cells were treated for 48 h with vehicle (–) or IFN-α (1000 U/ml). Immunoprecipitation (IP) of cell lysates was carried out with anti-AIF antibody, followed by Western blotting with anti-ISG15 or anti-AIF antibody. As a negative control, cell lysates were immunoprecipitated with preimmune IgG (IgG). The expression of ISG15 and AIF in cell extracts was identified by Western blotting with their corresponding antibodies. β-Actin and HSP90 served as the equal protein loading controls. The asterisk indicates IgG heavy chains. AIF, apoptosis-inducing factor; HEK293; human embryonic kidney 293; tAIF, truncated AIF.

ISGylated band with a size of approximately 90 kDa from full-length AIF was detected in the presence of multiple components of the ISG15-conjugating system, which was speculated to be derived from a mono-ISG15 conjugation product. However, two ISGylation bands with sizes of approximately 80 kDa and 110 kDa, respectively, were formed from tAIF, which matched the sizes of mono- and di-ISG15 (or two mono-ISG15) conjugation products (Fig. 1*A*). In addition, these ISGylated bands from full-length AIF and tAIF were not observed when the cells were coexpressed with the conjugation-deficient ISG15-AA mutant, where the C-terminal Gly-Gly residues were substituted with Ala-Ala as a negative control (Fig. 1*A*). To verify the ISGylation of tAIF and the pattern and size of their ISG15-conjugated bands, the cells were cotransfected with a plasmid encoding V5-His-tagged tAIF alone or with a plasmid encoding FLAG-tagged ISG15-GG or ISG15-AA, followed by coimmunoprecipitation (co-IP) of cell lysates with anti-V5 antibodies. Immunoblotting of anti-V5 immunocomplexes with anti-FLAG antiserum revealed two ISGylated tAIF bands with mono- and di-ISG15 conjugation products in the presence of WT ISG15, whereas these bands were not formed with the conjugation-defective ISG15-AA mutant (Fig. 1*B*). The multiple conjugation of tAIF with ISG15 was further confirmed by the finding that these two bands were missing after incubation with UBP43, a de-ISGylation enzyme (Fig. 1*C*). Unlike ubiquitin and ubiquitination, neither conjugation of poly-ISG15 chains to target proteins nor specific ISG15 interaction motifs have been reported to date (29). In addition, ISG15 has been reported to be conjugated as a monomer rather than a polymer to a lysine residue of a target protein (30). Based on these reports, the results from our *in vitro* experiments indicated that tAIF is conjugated by multiple ISG15 molecules.

Previous reports have shown that treatment with type I IFNs promotes the accumulation of ISG15 as well as its conjugating system, including E1, E2, and E3, subsequently increasing the covalent conjugation of ISG15 to its target protein (18). Based on this and our previous study showing that stimulation of A549 cells with type I IFN induced the ISGylation of multiple proteins (28), we next determined whether AIF could be ISGylated in A549 cells in response to IFN-α treatment. After A549 cells were left untreated or stimulated with IFN-α, co-IP of cell lysates revealed that endogenous AIF was ISGylated (Fig. 1*D*). As shown in Figure 1*D*, IFN-α treatment induced significantly increased expression of ISG15 in A549 cells, which is consistent with a previous finding (28). In addition, IFN-α treatment induced the formation of a single AIF band with a size of approximately 80 kDa, which was speculated to match the size of the mono-ISGylated truncated AIF band. Collectively, these data suggested that endogenous and truncated AIF could be targets of mono-ISGylation in response to IFN-α in A549 cells. Thus, the discrepancy in the ISGylation pattern of tAIF (*i.e.*, the detection of two ISGylated tAIF bands in Fig. 1, *A*–*C*) could be due to the overexpression of ISG15 protein leading to excessive ISGylation. Similar to the present data, we previously reported that overexpression of SUMO protein, another UBL modifier, caused excessive SUMOylation of targets based on *in vitro* experiments (31).

ISG15 E3 ligase HERC5 specifically promotes the ISGylation of tAIF

We next tried to identify the specific E3 ligase(s) that mediate the ISGylation of tAIF. To date, three E3 ligases have been identified to catalyze the ISG15-conjugating reaction to target: HERC5, EFP, and HHARI (16). HEK293 cells were cotransfected with plasmids encoding two components of the ISG15-conjugating system, UBE1L (E1) and UbcH8 (E2), V5-His-tagged tAIF, or each of the three E3 ligases, including FLAG-HERC5, Myc-EFP, or FLAG-HHARI, alone or in combination. Immunoprecipitation analyses showed that the presence of WT HERC5 enhanced the ISGylation of tAIF (Fig. 2*A*), whereas this effect was not observed in the presence of the catalytic-inactive HERC5-C994A mutant (Fig. 2*A*). Furthermore, the two ISGylation bands of tAIF disappeared when the cells were transfected with *HERC5*-siRNA (Fig. 2*B*). In contrast to the effect of HERC5, ISGylation of tAIF was unaffected by EFP or HHARI (Fig. 2, *D* and *E*). Moreover, we determined whether HERC5 acts as an ISG15 E3 ligase for endogenous AIF in A549 cells. After cells were transfected with HERC5-WT or HERC5-C994A, co-IP of cell lysates revealed that the ISGylation of endogenous AIF was significantly increased in the presence of HERC5-WT but not with HERC5-CA (Fig. 2*C*). These results suggested that HERC5, but not EEP or HHARI, acts as an ISG15 E3 ligase of tAIF. To further examine whether tAIF interacts with HERC5 in the absence of the ISG15-conjugating system, HEK293 cells were cotransfected with plasmids encoding V5-His-tagged truncated AIF or FLAG-HERC5 alone or together. As shown in Figure S1*A*, the co-IP assay further revealed that truncated AIF does not interact with HERC5 in resting cells. However, IFN-α treatment in A549 cells triggered considerable induction of HERC5. In addition, the binding of AIF to HERC5 was observed in A549 cells treated with IFN-α (Fig. S1*B*). These data demonstrate that HERC5 specifically promotes the ISGylation of tAIF.

Identification of ISGylation sites in tAIF

ISG15 has been reported to be conjugated as a monomer to a lysine residue of a target protein (30). Since only one band of endogenous AIF ISGylation was detected in A549 cells, we hypothesized that a single lysine residue in tAIF would be primarily modified by ISG15. To test this possibility, we next attempted to map which lysine residue of tAIF that is potentially modified by ISG15. To screen the ISGylation site within tAIF, we initially selected the most conserved lysine residues among species. The tAIF complementary DNA clone used in the present study was from the rat *Rattus norvegicus*, in which the N-terminal 101 amino acids were truncated, and there are a total of 31 lysine residues fully conserved between rats and humans. First, we generated a total of 31 tAIF mutants, in which 31 lysine residues were individually substituted with arginine (Fig. S2*A*). Unexpectedly, co-IP analyses revealed that

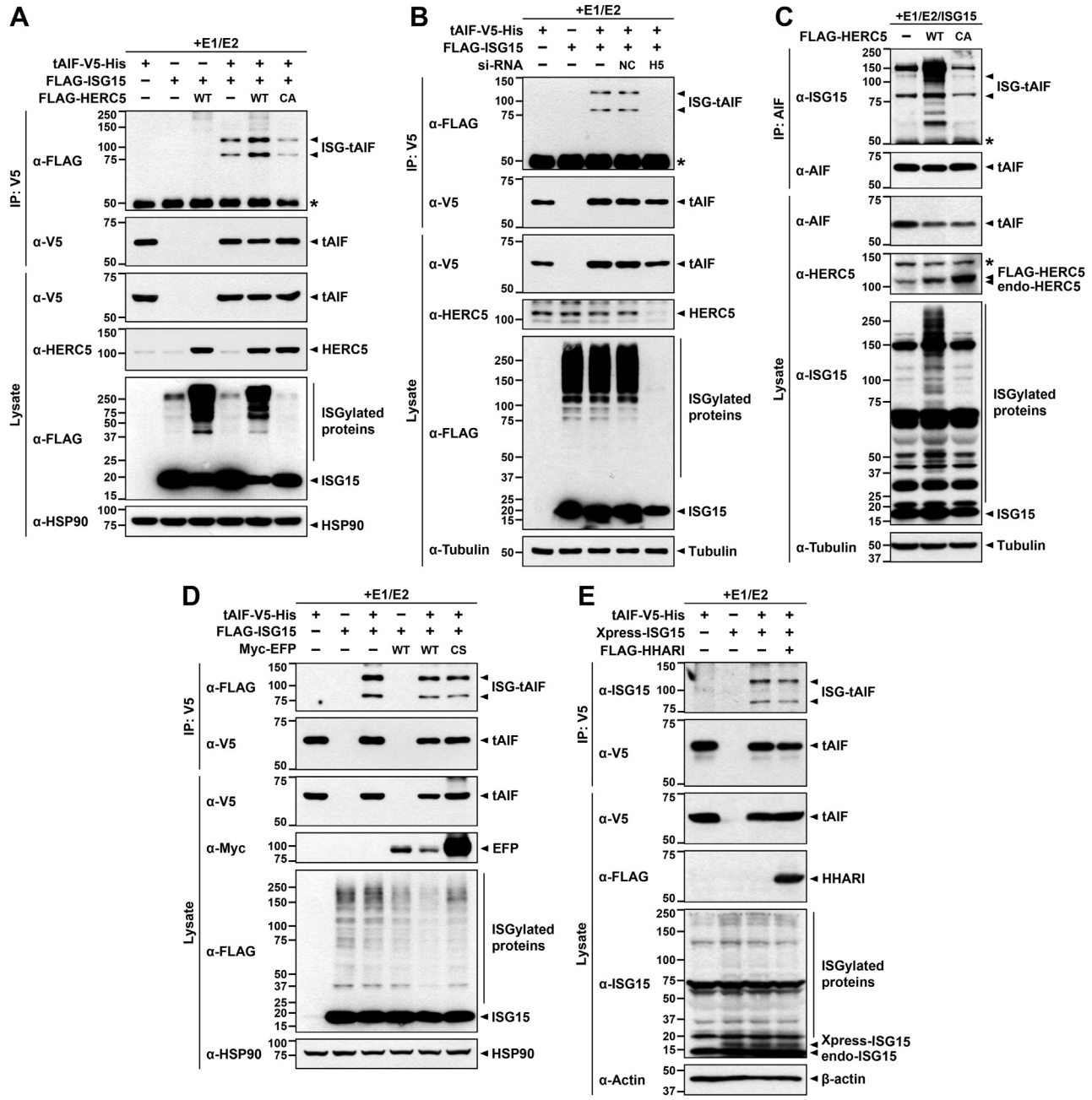

Figure 2. The ISG15 E3 ligase HERC5 specifically promoted the ISGylation of tAIF. *A*, where specified, HEK293 cells were transfected for 24 h with plasmids encoding E1, Myc-E2, tAIF-V5-His, FLAG-ISG15-WT, FLAG-HERC5-WT, or its catalytically inactive mutant (FLAG-HERC5-CA) alone or in combination. Cell lysates were immunoprecipitated using anti-V5 antibody, followed by Western blotting with anti-FLAG or anti-V5 antibody. *B*, HEK293 cells were transfected for 48 h with plasmids encoding E1, Myc-E2, tAIF-V5-His, FLAG-ISG15-WT, nonspecific scrambled control siRNA (NC), or *HERC5*-siRNA (H5) alone or in combination. Cell lysates were immunoprecipitated, followed by Western blotting with anti-FLAG or anti-V5 antibody. *C*, A549 cells were transfected for 24 h with plasmids encoding E1, Myc-E2, FLAG-ISG15-WT, FLAG-HERC5-WT, or FLAG-HERC5-CA alone or in combination. Cell lysates were immunoprecipitated using anti-AIF antibody, followed by Western blotting with anti-ISG15 or anti-AIF antibody. *D*, HEK293 cells were transfected for 24 h with plasmids encoding E1, Myc-E2, tAIF-V5-His, FLAG-ISG15-WT, FLAG-HERC5-WT, Myc-EFP-WT, or its catalytically inactive mutant (Myc-EFP-CS), alone or in combination. Cell lysates were immunoprecipitated, followed by Western blotting with anti-FLAG or anti-V5 antibody. *E*, HEK293 cells were transfected for 24 h with plasmid encoding E1, Myc-E2, tAIF-V5-His, Xpress-ISG15-WT, or FLAG-HHARI-WT alone or in combination. Cell lysates were immunoprecipitated, followed by Western blotting with anti-ISG15 or anti-V5 antibody. Tubulin, β-actin, and HSP90 served as the equal protein loading controls. The asterisk indicates IgG heavy chains. AIF, apoptosis-inducing factor; HEK293; human embryonic kidney 293; tAIF, truncated AIF.

all of these tAIF mutants failed to show any remarkable reduction in the extent of ISGylation compared to that observed in WT tAIF (Fig. S2*B*). These results implied that several sites in the tAIF could be randomly modified by ISG15 as a monomer rather than a single and fixed lysine residue.

AIF was previously reported to be a target of nondegradative ubiquitination at the K254 residue (in rat AIF, corresponding to K255 in human AIF) (12), and structural analysis of AIF protein revealed that the K473 and K243 residues are located close to K254 as well as at the surface of the protein. Similarly,

two additional lysine sites located around the groove region and close to each other were selected through structural analysis of AIF for identifying the candidate target of ISGylation and substituted with arginine. Therefore, three additional constructs encoding tAIF mutants were generated: the tAIF-3KR-1 mutant, in which the K243, K254, and K473 residues are substituted with arginine; the tAIF-3KR-2 mutant with point mutations at K230R, K231R, and K407R; and the tAIF-3KR-3 mutant with substitutions at K277R, K286R, and K295R (Fig. S2*C*). Co-IP analyses of these mutants revealed that the extent of tAIF-ISGylation was not significantly reduced compared to that of WT tAIF (Fig. S2*D*). In addition, we attempted to create several different tAIF mutants in which multiple lysine groups were substituted with arginine in various combinations and tested the effects of the mutations on ISGylation. However, no such effects were observed (data not shown).

Finally, the tAIF-K0 mutant was produced as a control, in which all 31 lysine groups within the protein were substituted with arginine. Despite the removal of all available lysine groups, the ISGylated bands of this tAIF-K0 mutant were still detected (Fig. S2*E*). From these data, we speculated that ISG15 modifies tAIF at amino acids other than lysine. Supporting this hypothesis, there have been several reports indicating that cysteine can also be modified by ISG15 (32, 33), although ISG15 mainly prefers to conjugate at lysine sites.

Next, we examined the validity of the hypothesis and if that is the case tried to identify the ISG15-targeting cysteine site(s) within the AIF through the mutagenesis analysis. As there are three cysteine residues in tAIF (C255, C316, and C440; Fig. S2*A*), total 14 tAIF mutants were generated in which two group of each seven mutants were produced using tAIF-WT and tAIF-K0 as s template, separately (Fig. 2, *F* and *G*). The seven point mutants of tAIF in each group were made by the substitution of three Cys residues with Ala in a single, double, or triple sites individually or together (Fig. 2, *F* and *G*). We then examined whether each mutant was still ISGylated. Unexpectedly, co-IP analyses revealed that the extent of ISGylation of all those 14 AIF mutants was not significantly reduced compared to that of tAIF-WT or tAIF-K0, respectively (Fig. 2, *F* and *G*). These results indicated that ISGylation of tAIF did not occur on Lys or Cys residue but on the novel site(s) that are not highly conserved.

ISGylation of AIF is induced by etoposide treatment in A549 cell

It is well known that mitochondrial AIF is truncated and released into the cytosol during apoptotic cell death under induction by various toxic signals such as DNA-damaging agents, kinase inhibitors, irradiation, and reactive oxygen species (3). Besides type I IFN, ISG15 is also induced by various cytotoxic stimuli, including viral infection, lipopolysaccharide, camptothecin, and etoposide (27). Based on these reports, we next investigated the stimuli that induce the ISGylation of apoptotic AIF in A549 cells among four toxic reagents tested: camptothecin (34), etoposide (27), MNNG (10), and staurosporine (35). Western blot analysis revealed that ISG15 was remarkably induced by etoposide and camptothecin in A549 cells but not by MNNG or staurosporine (Fig. 3*A*). As shown in Figure 3*B*, the maximal induction of ISG15 was obtained at 36 or 24 h with 50 or 100 μM etoposide, whereas it was reached at 24 h with 1 or 5 μM camptothecin (data not shown).

We then determined whether the ISGylation of tAIF was induced by etoposide or camptothecin. As shown in Figure 3*C*, HEK293 cells were cotransfected with ISG15-conjugating components and tAIF and then left untreated or stimulated with etoposide. Immunoblotting analysis of the samples showed that overexpression of HERC5 promoted total ISGylation levels in cell lysates as a control, and ISGylation was greatly enhanced under this condition with further etoposide stimulation. In addition, an immunoprecipitation assay confirmed the ISGylation of tAIF under these conditions, which significantly increased in the presence of HERC5. Moreover, ISGylation of tAIF was further increased when the cells were treated with etoposide (Fig. 3*C*). The same pattern of tAIF-ISGylation was observed in response to camptothecin treatment (Fig. S3*A*). Notably, under this condition of an excessive ISG15-conjugating system (*i.e.*, HERC5 overexpression plus etoposide treatment), slightly upshifted forms of V5-tAIF were clearly detected by immunoblot analysis with anti-V5 IgG, which was consistent with the presence of ISGylated tAIF bands detected in co-IP analysis (Fig. 3*C*). The same pattern of bands has been reported in many other studies (36–38). Furthermore, endogenous AIF of A549 cells was ISGylated upon treatment with etoposide or camptothecin (Figs. 3*D* and S3*B*). Etoposide treatment caused an interaction between endogenous AIF and HERC5 in A549 cells, although there was no binding detected in resting cells (Fig. 3*E*).

Finally, we examined whether the truncated form of endogenous AIF was actually generated when A549 cells were treated with etoposide. When cells were treated with etoposide alone, the endogenous tAIF level was detected but at a very low level making it difficult to observe (Fig. 3*F*). However, when the cells were cotreated with etoposide and the proteasome inhibitor MG132, the endogenous tAIF level was greatly increased compared with that detected under treatment of etoposide alone. As a control, when cells were treated with MG132 alone, there was no change in tAIF levels (Fig. 3*F*). Similar results were observed when camptothecin was used (Fig. S3*C*). These findings confirmed that endogenous tAIF induced by etoposide and camptothecin is subjected to proteasomal degradation, explaining why it is difficult to detect endogenous tAIF by Western blot analysis.

Collectively, these data suggest that treatment of A549 cells with DNA-damaging agents such as etoposide and camptothecin specifically triggered the ISGylation of tAIF.

ISGylation increases polyubiquitination of tAIF mainly through K6-linkage

We next investigated whether ISGylation affects the biochemical and functional properties of AIF. Our previous

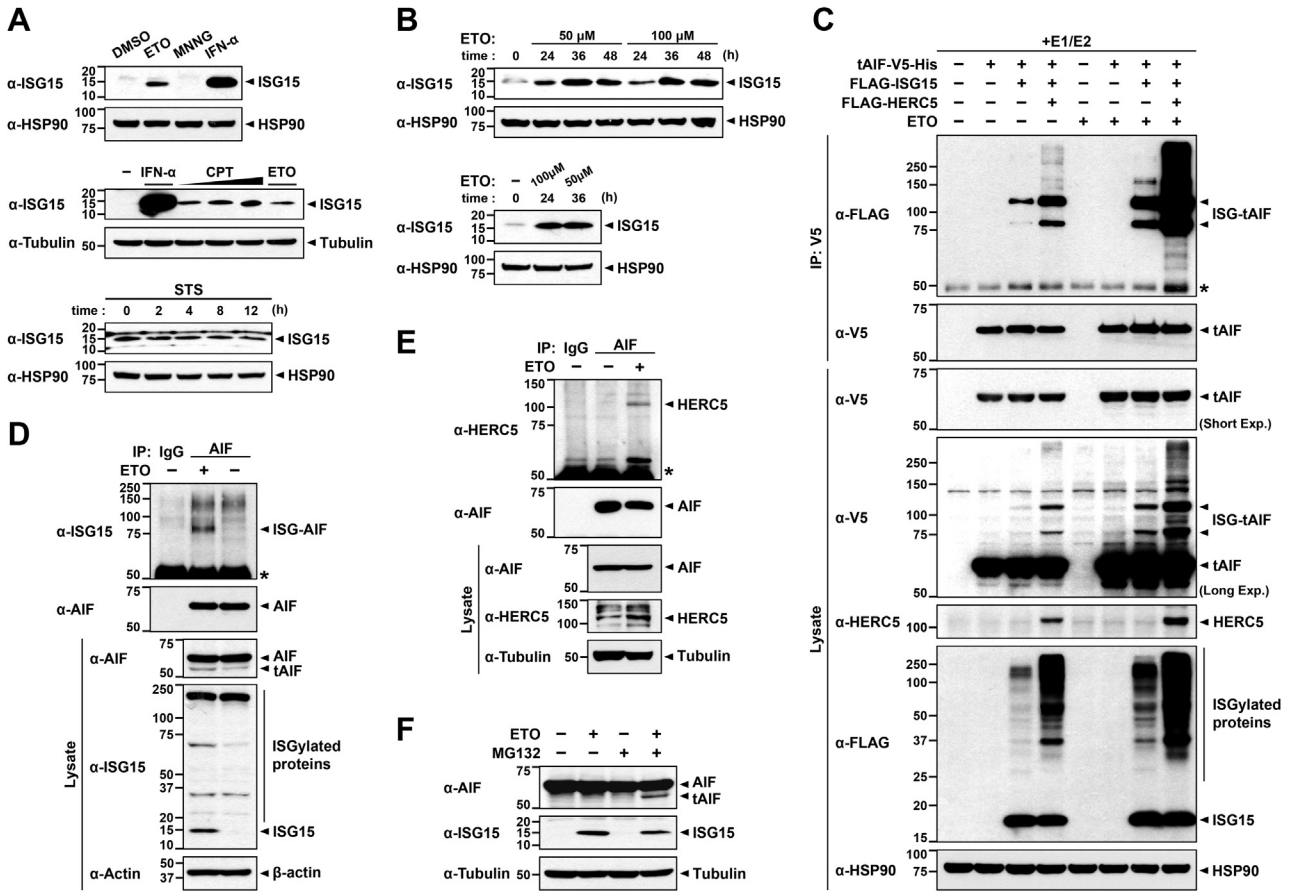

Figure 3. Treatment of A549 cells with etoposide triggered the ISGylation of tAIF. *A*, where indicated, A549 cells were treated for 24 h with vehicle (DMSO), etoposide (ETO, 100 μM), or interferon-α (IFN-α, 1000 U/ml), respectively. In the case of MNNG, the cells were treated with 0.5 mM MNNG for 15 min, washed with PBS, and further incubated for an additional 14 h (upper panel). A549 cells were treated for 24 h with vehicle (–), etoposide (100 μM), IFN-α (1000 U/ml), or camptothecin (CPT; 0.25, 1, or 2.5 μM), respectively (middle panel). A549 cells were treated for the indicated times with vehicle (–) or 1 μM staurosporine (STS, bottom panel). All cell lysates were immunoblotted with the indicated antibodies. *B*, A549 cells were treated for the indicated times with 50 or 100 μM etoposide. Cell lysates were immunoblotted with the indicated antibodies. *C*, HEK293 cells were transfected for 24 h with plasmids encoding UBE1L, HA-UbcH8, tAIF-V5-His, FLAG-ISG15-WT, or FLAG-HERC5-WT alone or in combination. Cells were then incubated with or without 100 μM etoposide for an additional 24 h. Cell lysates were immunoprecipitated using anti-V5 antibody, followed by immunoblotting with the indicated antibodies. *D*, A549 cells were treated for 24 h with vehicle (–) or 100 μM etoposide. Immunoprecipitation (IP) of cell lysates was carried out with anti-AIF antibody, followed by Western blotting with anti-ISG15 or anti-AIF antibody. As a negative control, cell lysates were immunoprecipitated with IgG. The expression of ISG15 and AIF in cell extracts was determined by Western blotting with their corresponding antibodies. *E*, A549 cells were treated for 24 h with vehicle (–) or 100 μM etoposide. IP of cell lysates was carried out with anti-AIF antibody, followed by Western blotting with anti-HERC5 or anti-AIF antibody. *F*, A549 cells were treated for 24 h with vehicle (–) or 100 μM etoposide. After replacing with fresh culture media, cells were then treated for an additional 4 h with vehicle (–) or 20 μM MG132. Cell lysates were immunoblotted with the indicated antibodies. As a negative control, cell lysates were immunoprecipitated with IgG. Tubulin, β-actin, and HSP90 served as the equal protein loading controls. The asterisk indicates IgG heavy chains. AIF, apoptosis-inducing factor; DMSO, dimethyl sulfoxide; HEK293; human embryonic kidney 293; MNNG, N-methyl-N-nitro-N′-nitrosoguanidine; tAIF, truncated AIF.

studies elucidated that ISGylation of target proteins affects polyubiquitination (27, 28). Thus, we first examined whether ISGylation affects the polyubiquitination or mono-ubiquitination of tAIF. HEK293 cells were transfected with plasmids encoding ISG15 conjugation components, including E1 and E2, FLAG-ISG15, or tAIF-V5-His alone or in combination to set the conditions for tAIF-ISGylation, and an immunoprecipitation assay of cell lysates with anti-V5 antibodies was performed. Immunoblotting of anti-V5 immunocomplexes with antiubiquitin antibodies revealed that the polyubiquitination of tAIF was enhanced to a certain degree in the presence of ISG-WT (Fig. 4*A*). However, this effect was not observed with ISG-AA (Fig. 4*A*). Moreover, the extent of tAIF polyubiquitination was further enhanced by HERC5-WT, whereas it was almost abolished by the catalytically inactive HERC5-CA mutant (Fig. 4*B*). Similarly, treatment of A549 cells with etoposide, which was found to promote tAIF-ISGylation, greatly increased the polyubiquitination level of endogenous AIF (Fig. 4*C*). These results suggested that ISGylation promotes the polyubiquitination of tAIF. This was further confirmed by the finding that transfection of A549 cells with *HERC5*-specific siRNA decreased the polyubiquitination level of endogenous AIF that was induced by etoposide treatment, which reached the control level (Fig. 4*D*). To determine the specific lysine-linkage type(s) in the poly-ubiquitin chain of ISGylated-tAIF, HEK293 cells were transfected with tAIF-V5-His and ISG15 conjugation components alone or together with one of several plasmids encoding WT ubiquitin or its mutants (Fig. 4*E*). These include the ubiquitin K6, K11, K27, K29, K33, K48, and K63 mutants, and the

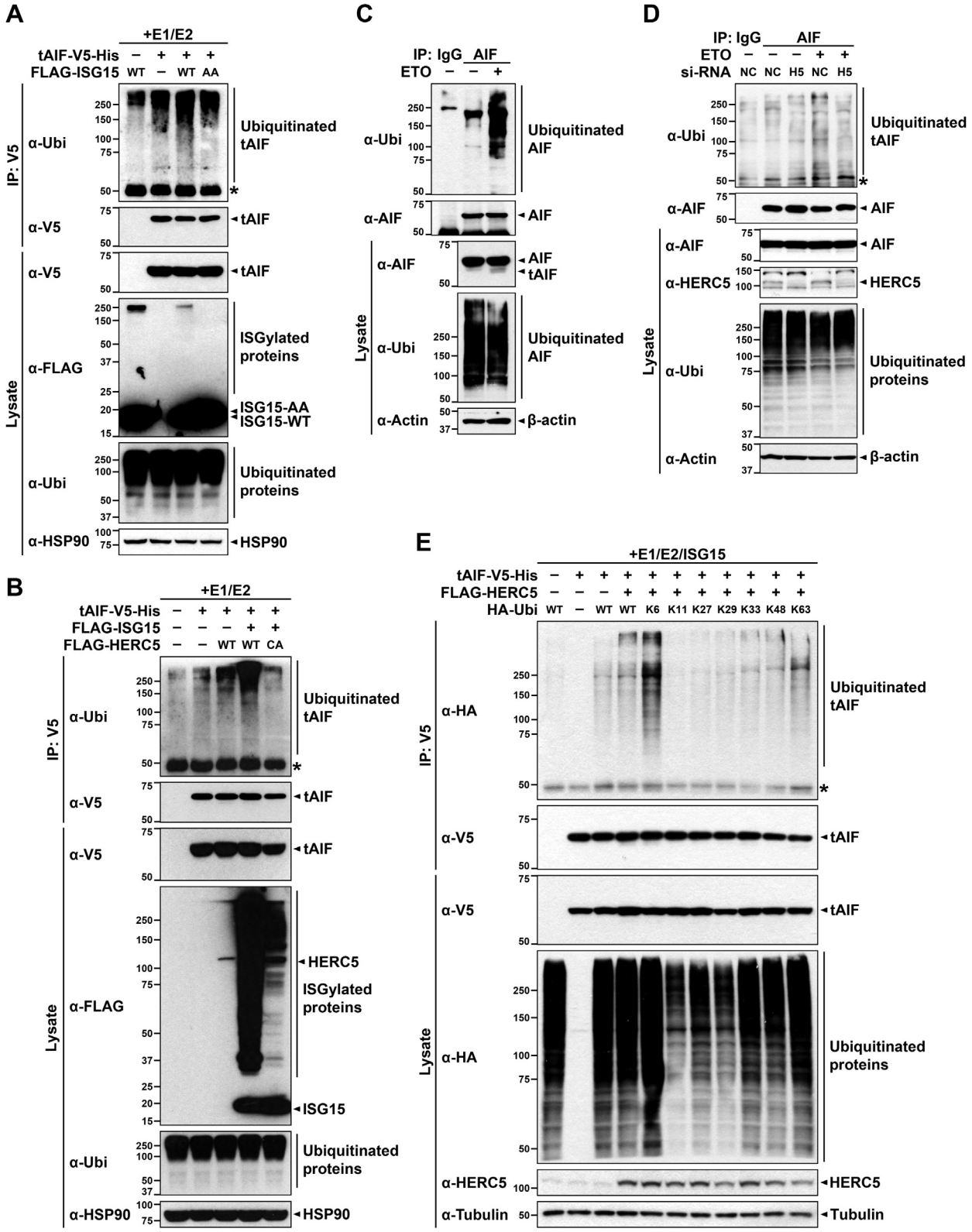

Figure 4. ISGylation increased the K6-linked polyubiquitination of tAIF. *A*, HEK293 cells were transfected for 24 h with plasmids encoding UBE1L, Myc-UbcH8, tAIF-V5-His, FLAG-ISG15-WT, or FLAG-ISG15-AA, alone or in combination. Cell lysates were immunoprecipitated using an anti-V5 antibody, followed by immunoblotting with the indicated antibodies. *B*, HEK293 cells were transfected for 24 h with plasmids encoding UBE1L, Myc-UbcH8, tAIF-V5-His, FLAG-ISG15-WT, FLAG-HERC5-WT, or FLAG-HERC5-CA, alone or in combination. Cell lysates were immunoprecipitated using an anti-V5 antibody, followed by immunoblotting with the indicated antibodies. *C*, A549 cells were treated for 24 h with vehicle (–) or 100 μM etoposide. Immunoprecipitation (IP) of cell lysates was carried out with anti-AIF antibody, followed by Western blotting with antiubiquitin (Ubi) or anti-AIF antibody. *D*, A549 cells were transfected for 48 h with nonspecific scrambled control siRNA (NC) or *HERC5*-siRNA (H5). Cells were then incubated with or without 100 μM etoposide for an additional 24 h. Cell lysates were immunoprecipitated using an anti-AIF antibody, followed by immunoblotting with the indicated antibodies. As a negative control, cell lysates were immunoprecipitated with IgG. The expression of HERC5 and AIF in cell extracts was determined by Western blotting with their

indicated number of each ubiquitin mutant denoted the lysine residue to remain intact among the seven total lysine residues, while the other six residues were mutated to arginine. Among these mutants, tAIF was polyubiquitinated through K6-linkage of the lysine residue under the condition of ISG15 conjugation; this linkage is known to be proteasome mediated degradation independent but is mostly involved in DNA repair (Fig. 4*E*).

Overall, these data suggest that ISGylation increases the polyubiquitination of AIF through K6-ubiquitin linkage.

ISGylation increases the half-life of tAIF

Next, we examined whether ISGylation affects the protein stability of tAIF. To determine if ISGylation regulates the half-life of tAIF, it was compared in the presence or absence (blockade) of HERC5 expression. *HERC5*-siRNA efficiently decreased the HERC5 expression level in A549 cells by 30% (Fig. 5*A*). Evaluation of the half-life of exogenous tAIF following treatment with cycloheximide revealed that tAIF protein was degraded much faster over 24 h in *HERC5*-knockdown cells compared to its degradation rate in control cells treated with nonspecific control siRNA (Fig. 5*B*). Similar results were also observed when UBP43 was overexpressed in A549 cells, which greatly reduced the half-life of exogenous tAIF by 2.3-fold (Fig. 5, *C* and *D*). Moreover, the half-life of exogenous tAIF was greatly reduced in the presence of the conjugation-defective ISG-AA mutant, with a reduction of 48%, compared with that of cells with ISG15-WT (Fig. 5, *E* and *F*). When we further measured the half-life of endogenous tAIF, it was not much affected under etoposide treatment, compared with that of control cells without any treatment (Fig. 5*G*). However, *HERC5*-knockdown followed by etoposide treatment caused a significant reduction in the half-life of endogenous tAIF. In addition, the relative tAIF level was significantly increased by etoposide and decreased again by *HERC5*-knockdown. Taken together, these results suggested that ISGylation increases the half-life of tAIF.

ISGylation promotes the cytosolic release of tAIF and its nuclear transport upon toxic stimuli

As described previously, when cells are exposed to apoptotic signals, including etoposide, mitochondrial AIF is released into the cytoplasm and ultimately translocated to the nucleus, triggering apoptosis (3). Therefore, we examined whether ISGylation has an effect on the intracellular localization of AIF following treatment with etoposide. After A549 cells were treated with etoposide for different times, cell lysates were sequentially fractionated into four subcellular fractions: cytoplasmic (Cyto), membrane organelle (Memb), soluble nuclear (Sol-Nucl), and chromatin-bound nuclear (Chr-Nucl) extracts. Immunoblotting analyses of these fractions revealed that the amount of tAIF protein was increased gradually under etoposide treatment in all fractions, reaching the maximum value at 24 h. In particular, the amount of tAIF protein is abundant in the cytosol and soluble nuclear fraction, whereas it is relatively small in the membrane and chromatin-bound nuclear fraction. Moreover, the expression of ISG15 in cells treated with etoposide for up to 12 h was induced at a similar level to that of control cells without any stimuli. However, cells treated with etoposide for more than 24 h displayed much stronger induction of ISG15 than the control group (Figs. 6*A* and 3*B*). Unfortunately, the induction of ISG15 could not be clearly assessed in chromatin-bound nuclear fraction due to the presence of a strong and putative nonspecific band exactly matched to the size of ISG15. To further determine whether this protein band corresponds to either ISG15 or other nonspecific band, the same experiment was repeated in the presence of control siRNA or *ISG15*-siRNA. As shown in Figure S4, the steady-state and etoposide-induced ISG15 levels were efficiently blocked by *ISG15*-siRNA in cytosolic fraction, whereas this effect was not seen in chromatin-bound nuclear fraction. These results indicated that the 15 kDa protein band in the chromatin-bound nuclear fraction was not the ISG15 but a nonspecific band whose identity was unknown. These results further suggest that, in order for the truncated AIF to be ISGylated, cellular treatment with etoposide for more than 24 h is required.

Accordingly, A549 cells were cotransfected with the plasmids encoding the ISG15 conjugation components in combination and then treated with 100 μM etoposide for an additional 24 h. The cell lysates were sequentially fractionated into four subcellular fractions, and co-IP analyses of these fractions revealed that ISGylation of AIF mainly occurred in the cytoplasm at a steady state under resting conditions (Fig. 6*B*). In contrast, when cells were treated with etoposide, ISGylation was dramatically increased not only in the cytoplasm but also in the soluble and chromatin-bound nuclei (Fig. 6*B*). Moreover, we found a greater increase in ISGylation of AIF in soluble nuclear fraction than in chromatin-bound nuclear fraction (Fig. 6*B*).

To further characterize the effect of ISGylation on the subcellular localization of tAIF, the colocalization of endogenous AIF and ISG15 was examined in A549 cells. As shown in Figure 6*C*, AIF was mainly colocalized with ISG15 at a steady state in the cytoplasm. Upon etoposide treatment, colocalization of AIF and ISG15 was increased not only in the cytoplasm but also in the nucleus (Fig. 6*C*). Consistently, similar results were obtained in response to camptothecin treatment (Fig. S5*A*). To verify the intracellular localization of covalently conjugated AIF by ISG15, the actual interaction between AIF and ISG15 was measured using a proximity ligation assay (PLA) in A549 cells. Consistent with the previous results, the PLA showed that ISGylated AIF barely occurred in the normal state (Fig. 6*D*). However, when the cells were treated with

corresponding antibodies. *E*, where specified, HEK293 cells were transfected for 24 h with plasmids encoding ISG15-conjugating components, tAIF-V5-His, FLAG-HERC5, HA-tagged WT ubiquitin (HA-Ubi-WT), or the mutant in which six lysine residues except for the numbered lysine site (K6, K11, K27, K29, K33, K48, or K63) were replaced with arginine, alone or in combination. Cell lysates were immunoprecipitated using anti-V5 antibody, followed by immunoblotting with the indicated antibodies. Tubulin, β-actin, and HSP90 served as the equal protein loading controls. The asterisk indicates IgG heavy chains. AIF, apoptosis-inducing factor; HEK293; human embryonic kidney 293; tAIF, truncated AIF.

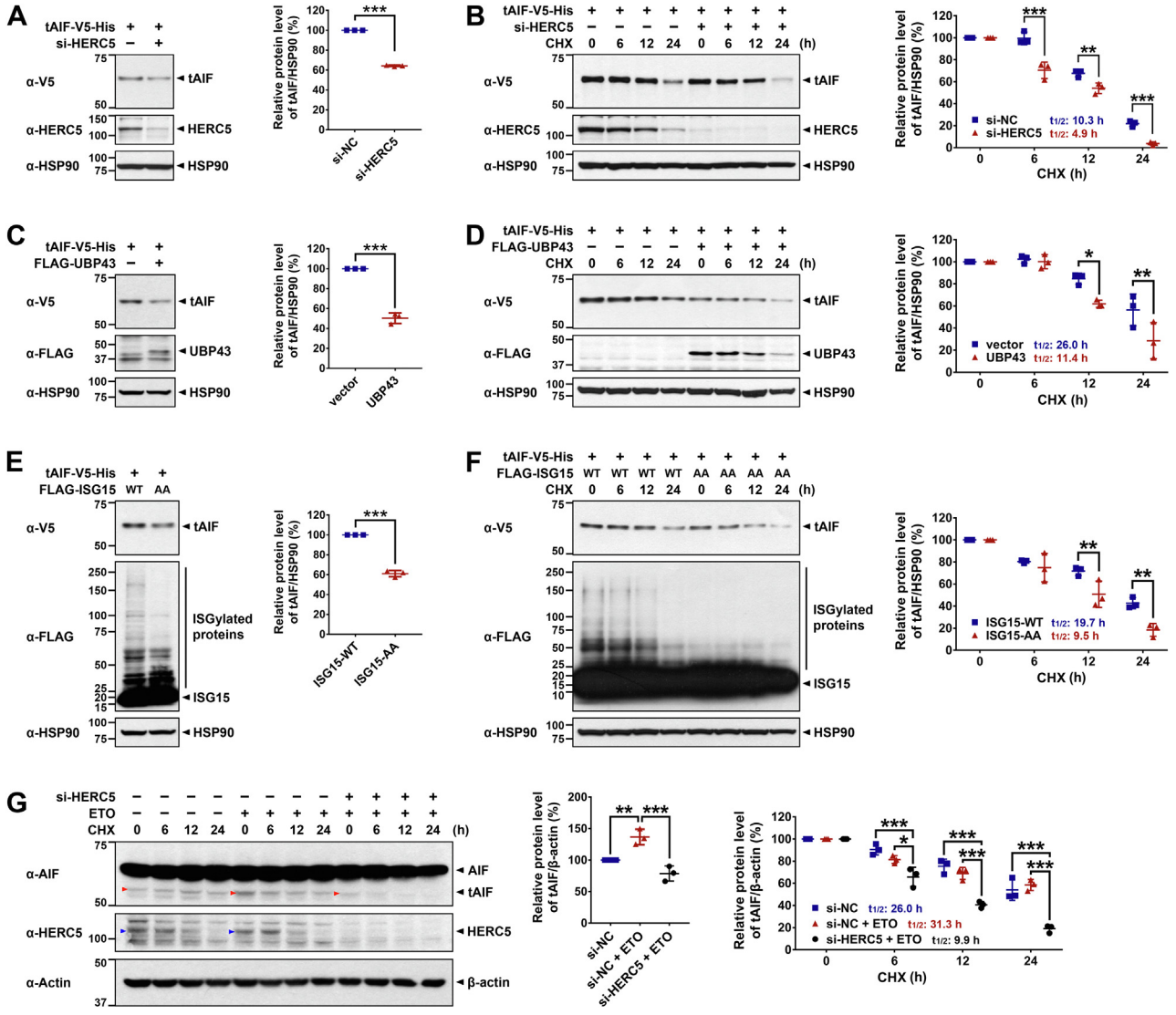

Figure 5. ISGylation increased the half-life of tAIF. *A*, A549 cells were transfected for 48 h with a plasmid encoding tAIF-V5-His, nonspecific scrambled control siRNA (–), or *HERC5*-siRNA, alone or in combination. Cell lysates were immunoblotted with the indicated antibodies. Relative protein levels of tAIF compared with HSP90 were quantified, and the data are presented as the mean ± SEM of three independent experiments (***$p < 0.001$). *B*, A549 cells were transfected for 48 h with nonspecific control scrambled siRNA (–), *HERC5*-siRNA, or a plasmid encoding V5-His-tagged tAIF. Cells were then treated for the indicated times with 50 μg/ml cycloheximide (CHX) and cell lysates were immunoblotted with the indicated antibodies. Relative protein levels of tAIF compared with HSP90 were quantified and the data are presented as the mean ± SEM of three independent experiments (**$p < 0.01$; ***$p < 0.001$). *C*, A549 cells were transfected for 24 h with plasmids encoding V5-His tagged tAIF alone or together with FLAG-UBP43. Cell lysates were immunoblotted with the indicated antibodies. Relative protein levels of tAIF compared with HSP90 were quantified and the data are presented as the mean ± SEM of three independent experiments (***$p < 0.001$). *D*, A549 cells were transfected for 24 h with plasmids encoding V5-His-tagged tAIF, alone or together with FLAG-UBP43. The cells were then treated for the indicated times with 50 μg/ml CHX and cell lysates were immunoblotted with the indicated antibodies. Relative protein levels of tAIF compared with HSP90 are quantified and the data are presented as the mean ± SEM of three independent experiments (*$p < 0.05$; **$p < 0.01$). *E*, A549 cells were transfected for 24 h with plasmids encoding V5-His-tAIF, alone or together with FLAG-ISG15-WT or FLAG-ISG15-AA. Cell lysates were immunoblotted with the indicated antibodies. Relative protein levels of tAIF compared with HSP90 were quantified and the data are presented as the mean ± SEM of three independent experiments (***$p < 0.001$). *F*, A549 cells were transfected for 24 h with plasmids encoding V5-His-tAIF alone or together with FLAG-ISG15-WT or FLAG-ISG15-AA. The cells were then treated for the indicated times with 50 μg/ml CHX and cell lysates were immunoblotted with the indicated antibodies. Relative protein levels of tAIF compared with HSP90 were quantified and the data are presented as the mean ± SEM of three independent (**$p < 0.01$). *G*, where specified, A549 cells were transfected for 48 h with nonspecific scrambled control siRNA (–) or *HERC5*-siRNA and then treated for the indicated times with 50 μg/ml CHX or/and 100 μM etoposide (ETO) for 24 h. All samples were treated for 6 h with 20 μM MG132. Cell lysates were immunoblotted with the indicated antibodies. Relative protein levels of endogenous tAIF compared with β-actin were quantified and the data are presented as the mean ± SEM of three independent (*$p < 0.05$; **$p < 0.01$; ***$p < 0.001$). β-Actin and HSP90 served as the equal protein loading controls. AIF, apoptosis-inducing factor; 293; tAIF, truncated AIF.

etoposide or camptothecin, the colocalization and interaction between ISG15 and AIF remarkably increased. Moreover, the extent of tAIF-ISGylation at the nuclear fraction increased, suggesting that ISGylation promotes the cytosolic release and nuclear translocation of tAIF (Figs. 6*D* and S5*B*). This hypothesis was further validated by an additional assay to determine whether HERC5 influences the interaction between AIF and ISG15 induced by etoposide and camptothecin and its change between the subcellular fractions. The PLA revealed that knockdown of *HERC5* significantly reduced the

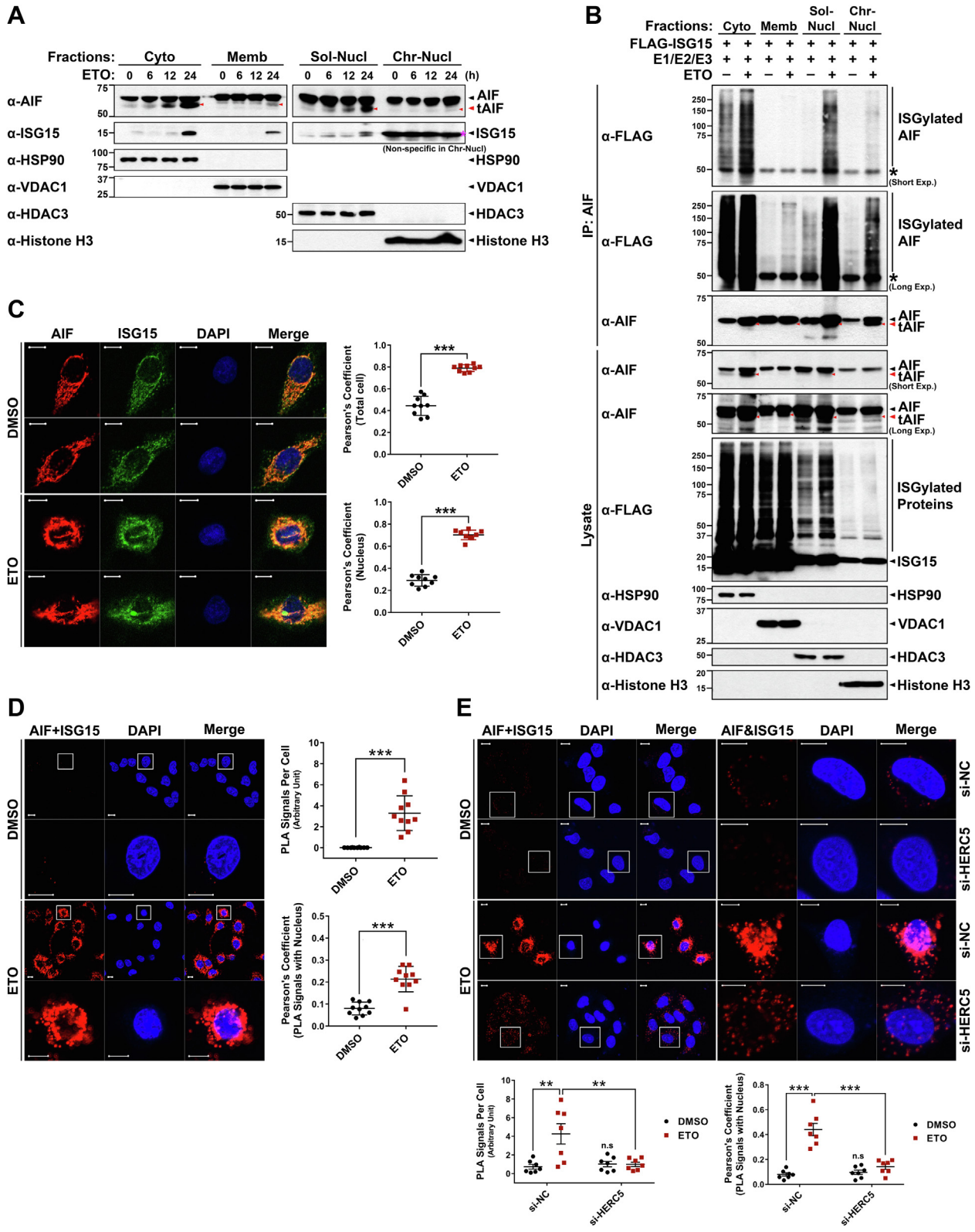

Figure 6. ISGylation promotes the cytosolic release and nuclear transport of tAIF upon etoposide treatment. *A* and *B*, all samples were treated for 6 h with 20 μM MG132. *A*, after A549 cells were treated with 100 μM etoposide for the indicated times, cells were harvested, lysed, and fractionated into the cytoplasmic (Cyto), membrane organelle (Memb), soluble nuclear (Sol-Nucl), and chromatin-bound nuclear (Chr-Nucl) extracts. Cell lysates were then immunoblotted with the indicated antibodies. The asterisk indicated the nonspecific bands in the chromatin-bound nuclear fraction. *B*, A549 cells were transfected for 24 h with plasmids encoding UBE1L, HA-UbcH8, FLAG-ISG15-WT, and FLAG-HERC5-WT. Cells were then incubated without (DMSO) or with 100 μM etoposide (ETO) for 24 h. Cells were harvested, lysed, and fractionated into the cytoplasmic (Cyto), membrane organelle (Memb), soluble nuclear (Sol-Nucl), and chromatin-bound nuclear (Chr-Nucl) extracts. The samples were immunoprecipitated using an anti-AIF antibody, followed by immunoblotting with the indicated antibodies. HSP90, VDAC1, HDAC3, and histone H3 served as the respective markers for the cytoplasmic fraction, mitochondrial (membrane organelle) fraction, soluble nuclear fraction, and chromatin-bound nuclear fraction. *C*, A549 cells were treated for 24 h with 100 μM etoposide

ISGylation of AIF, as expected (Figs. 6*E* and S5*C*). In addition, ISGylation was significantly enhanced by etoposide or camptothecin treatment, but the blockade of *HERC5* expression further inhibited the nuclear translocation of ISGylated AIF compared with that in the control cells transfected with the control siRNA. (Figs. 6*E* and S5*C*).

Overall, these data indicated that ISGylation of AIF plays a vital role in the nuclear translocation of AIF upon treatment with etoposide or camptothecin.

HERC5-mediated ISGylation of tAIF promotes cell death following etoposide treatment

Finally, we investigated whether ISGylation influences tAIF-mediated cell death. As we previously reported that ISGylation is more likely to occur in A549 cells than in HEK293 cells, which are lacking some of its essential components (28), we examined the effect of tAIF-ISGylation on the cytotoxicity in HEK293 and A549 cell lines, respectively. As shown in Figure 7*A*, immunoblotting analysis verified that ectopically transfected tAIF and the components of ISG15 conjugating system, including ISG15, E1, E2, and E3, were properly expressed in HEK293 cells. Measurement of HEK293 cell viability using the lactate dehydrogenase (LDH) cytotoxicity assay revealed that cells treated with etoposide alone displayed cell death by ∼31% compared with mock-transfected control cells (Fig. 7*B*). In addition, HEK293 cells transfected with tAIF or the ISG15 conjugation system alone showed insignificant change in etoposide-induced cytotoxicity, compared to the control cells, respectively (Fig. 7*B*). When cells were cotransfected with tAIF and the ISG15 conjugating components followed by etoposide treatment, the cytotoxicity was increased by ∼14% from 31% of the control group to 45% (Fig. 7*B*). These results indicated that tAIF expression alone cannot exert a cytotoxic effect in HEK293 cells in which the ISG15 conjugating system does not exist. However, when an artificial environment was created in HEK293 cells to trigger the reactions of covalent ISG15 conjugation to their protein targets, the extent of cell death was considerably promoted following the etoposide-induced ISGylation of tAIF. Similarly, before performing the cytotoxicity assay in A549 cells, immunoblotting analysis confirmed that the expression of AIF and HERC5 was efficiently blocked by treatment with their siRNAs (Fig. 7*C*). Then, the measurement of A549 cell viability showed that etoposide treatment alone induced cell death by ∼85% in cells transfected with nonspecific control siRNA (Fig. 7*B*). However, A549 cells treated with *AIF*-siRNA showed a ∼5% decrease in etoposide-induced cytotoxicity compared with that of the control cells. These results indicated that AIF expression alone could exert a cytotoxic effect in A549 cells. Intriguingly, the knockdown of *HERC5* expression also reduced the cytotoxicity of etoposide by ∼7% compared to that of the control group. These results suggest that, similar to the silencing of AIF, the blockade of *HERC5* expression and subsequent inhibition of tAIF-ISGylation has a cytoprotective effect. Finally, when both *AIF*- and *HERC5*-specific siRNAs were cotransfected into cells followed by treatment with etoposide, the cytotoxicity of cells was attenuated in an additive manner compared with that of the cells transfected with either siRNA alone (Fig. 7*D*). Finally, to determine whether cell death induced by AIF-ISGylation and identified by LDH assay occurs through apoptosis, flow cytometry analysis was performed using Annexin V-FITC and propidium iodide (PI) staining. When the expression of *AIF* and *HERC5* was blocked simultaneously using their corresponding siRNAs, flow cytometry showed a reduction in apoptotic cell death by ∼18% compared with that of the control group (***$p < 0.001$, Fig. 7*E*). Taken together, these results suggest that AIF and HERC5 play essential roles in apoptotic A549 cell death. In addition, HERC5-mediated ISGylation of AIF promoted apoptosis upon etoposide treatment.

Discussion

In the present study, we demonstrated that tAIF is a novel target for ISG15 conjugation. However, when the bands of ISG15-conjugated tAIF were closely analyzed, there were some inconsistencies. For example, two major ISGylated bands were observed under the ectopic expression of ISGylation components corresponding to the size of multi-ISG15–conjugated tAIF (Figs. 1, *A* and *B* and 2). However, upon stimulation with IFN-α or DNA-damaging agents, only one ISGylated band of endogenous tAIF was detected (Fig. 1*D*), which corresponded to the size of the mono-ISG15–conjugated form. Moreover, multiple bands, including two major bands, were observed when ISG15 was excessively attached to tAIF, such as under the condition of *HERC5* overexpression and/or toxic reagent treatment (Figs. 3*C* and 5*C* and 6*A*). This phenomenon could be explained by the differential environment of target ISGylation, such as a physiologically low extent of or excessive conjugation. Several studies have reported that it is difficult to observe the ISGylation of endogenous target proteins (30, 36, 39). These studies explain the difficulty in detecting endogenous ISGylated proteins, presumably due to transient ISG15 conjugation to target proteins, as it is generally known that covalent ISG15 conjugation is immediately removed from the

before fixation. Representative confocal images of endogenous AIF (*red*) and ISG15 (*green*) immunostaining are shown. The scale bar represents 10 μm. The colocalization of AIF and ISG15 was analyzed by calculating Pearson's correlation coefficient with Image J software. Data are presented as the mean ± SEM of three independent experiments (n = 9; ***$p < 0.001$). *D*, A549 cells were treated for 24 h without (DMSO) or with 100 μM etoposide before fixation. Proximity ligation assays (PLAs) were performed with the primary antibodies of AIF and ISG15. Representative PLA images of endogenous ISGylated AIF (*red*) are shown. The scale bar represents 10 μm. The PLA signals were quantified using Image J software and depicted as a scatter plot. The colocalization of ISGylated AIF (*red*) and the nucleus (*blue*) was analyzed by calculating Pearson's correlation coefficient with Image J software. Data are presented as the mean ± SEM of three independent experiments (n = 10; ***$p < 0.001$). *E*, A549 cells were transfected for 48 h with the nonspecific control siRNA (si-NC) or *HERC5*-siRNA and treated for an additional 24 h with DMSO or etoposide (100 μM). PLA was performed as described in (*C*). Representative PLA images of endogenous ISGylated AIF (*red*) are shown. The scale bar represents 10 μm. The PLA signals were quantified using Image J software and depicted as a scatter plot. The colocalization of ISGylated AIF (*red*) and the nucleus (*blue*) was analyzed by calculating Pearson's correlation coefficient with Image J software. Data are presented as the mean ± SEM of three independent experiments (n = 7; *$p < 0.05$; **$p < 0.01$; ***$p < 0.001$; n.s, not significant). AIF, apoptosis-inducing factor; DMSO, dimethyl sulfoxide; tAIF, truncated AIF.

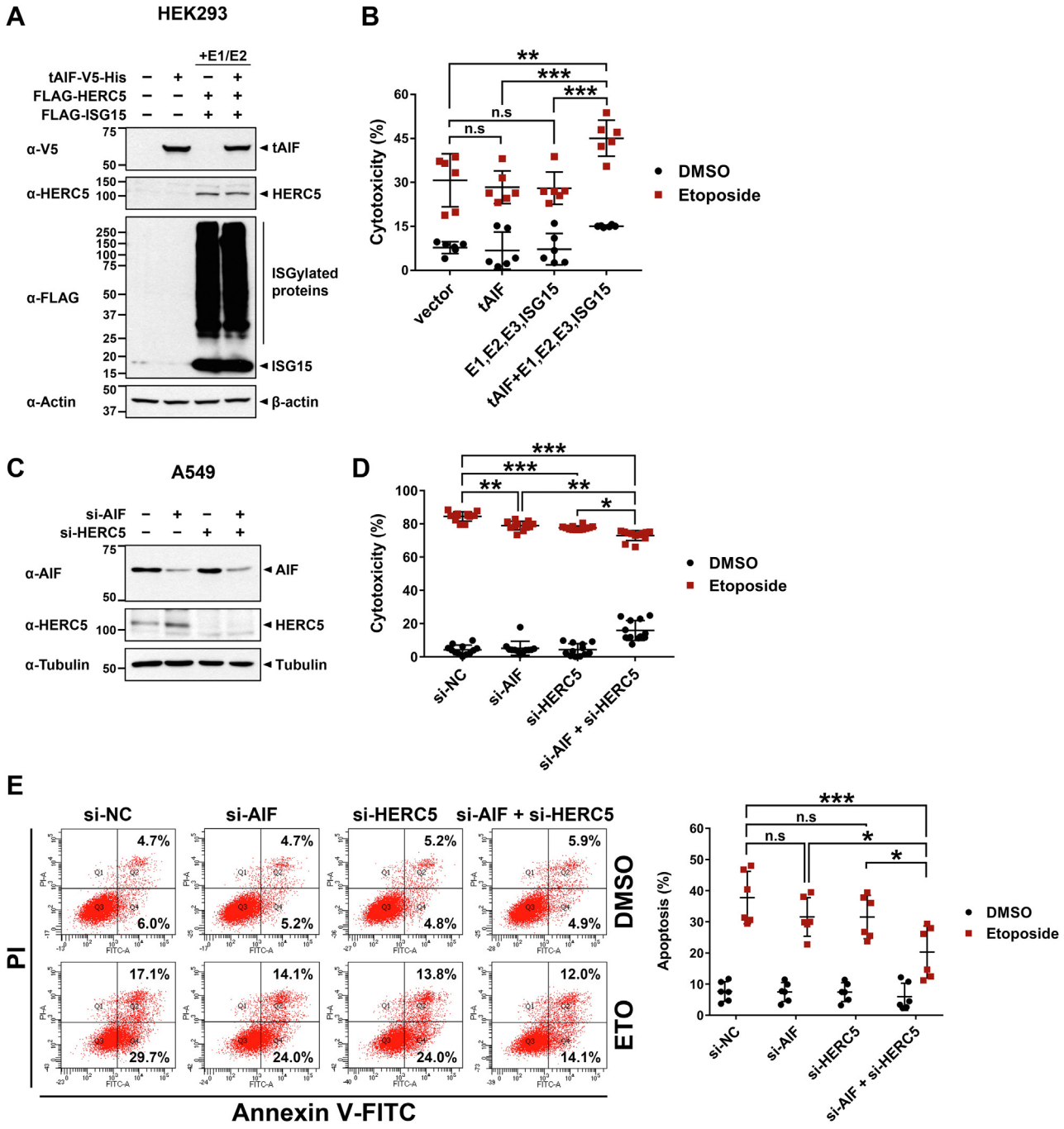

Figure 7. ISGylation promoted tAIF-induced cell death following etoposide treatment. *A*, HEK293 cells were transfected for 24 h with plasmids encoding UBE1L, Myc-UbcH8, FLAG-ISG15-WT, FLAG-HERC5-WT, or tAIF-V5-His, alone or in combination. Cell lysates were immunoblotted with the indicated antibodies. β-Actin served as a loading control. *B*, HEK293 cells were transfected for 24 h with plasmids encoding UBE1L, Myc-UbcH8, FLAG-ISG15-WT, FLAG-HERC5-WT, or tAIF-V5-His alone or in combination and treated for an additional 24 h with DMSO or etoposide (100 μM). Cell toxicity was measured using an LDH assay kit. Data are represented as the mean ± SEM of three independent experiments (n = 6; $^{**}p < 0.01$; $^{***}p < 0.001$). *C*, A549 cells were transfected for 48 h with nonspecific scrambled control siRNA (–), *HERC5*-siRNA, or *AIF*-siRNA. Cell lysates were immunoblotted with the indicated antibodies. Tubulin served as a loading control. *D*, A549 cells were transfected for 48 h with nonspecific control siRNA (si-NC), *AIF*-siRNA, or *HERC5*-siRNA and treated for an additional 24 h with DMSO or etoposide (100 μM). Cell toxicity was measured using an LDH assay kit. Data are represented as the mean ± SEM of four independent experiments (n = 12; $^{*}p < 0.05$; $^{**}p < 0.01$; $^{***}p < 0.001$). *E*, A549 cells were transfected for 48 h with nonspecific control siRNA (si-NC), *AIF*-siRNA, or *HERC5*-siRNA and treated for an additional 24 h with DMSO or etoposide (100 μM). The extent of apoptotic cell death was detected by flow cytometry. On the two-dimensional scatter diagram, Annexin V-FITC and PI are on the *x*- and *y*-axes, respectively. The second quadrant represents late apoptotic cells and the fourth quadrant represents early apoptotic cells. The diagram shown in this figure is representative of multiple experiments. The data are presented as a graph of the mean ± SEM of three independent experiments (n = 6; $^{*}p < 0.05$; $^{**}p < 0.01$; $^{***}p < 0.001$; n.s, not significant). AIF, apoptosis-inducing factor; DMSO, dimethyl sulfoxide; HEK293; human embryonic kidney 293; PI, propidium iodide; tAIF, truncated AIF.

target substrate by the ISG15-deconjugate enzyme USP18 (30, 36, 39). Moreover, we speculate that multiple bands might be generated due to the excessive ISGylation of tAIF accompanied by additional polyubiquitination (40). Similar to the present findings, we previously reported that covalent conjugation of SUMO protein, another member of the

ubiquitin-like modifier family, to its novel target produced double and triple SUMOylated forms, which were attributed to increased SUMO levels and consequent excessive SUMOylation (31, 41). More specifically, zinc finger protein 131 (ZNF131) is mono-SUMOylated at the Lys567 residue under physiological conditions using either endogenous SUMO1 or SUMO2/3. Nevertheless, overexpression of SUMO protein and SUMO E3 ligase UHRF2 generated di- and tri-SUMOylated forms of ZNF131 in HEK293 cells, which likely occurred because of increased SUMO levels and subsequent excessive SUMOylation. Similarly, multiple auto-SUMOylated UHRF2 bands were generated in cells overexpressing SUMO protein, whereas UHRF2 was mono-SUMOylated under physiological conditions using endogenous SUMO1.

Among the three ISG15 E3 ligases, we clarified that HERC5 mediates the ISGylation of tAIF. Although we observed that ISGylation was clearly promoted by HERC5, the interaction between tAIF and HERC5 was difficult to observe under normal resting conditions. Interestingly, the binding of tAIF to HERC5 was observed upon treatment with IFN-α, etoposide, or camptothecin, in which the ISG15 conjugation system was activated. According to a previous study, HERC5 mediates covalent ISG15 conjugation to another substrate, Parkin, in mammalian cells (27). Similar to the present findings, we could not detect the interaction between HERC5 and Parkin in the resting condition. Parkin specifically bound to WT HERC5 and its catalytically inactive mutant, when it was coexpressed with three components of the ISG15 conjugation system (27). These results indicated that the interaction between HERC5 and Parkin might be mediated by another unknown component. The present data support this hypothesis, further suggesting that the interaction between HERC5 and its target protein might be mediated by other unknown factor(s) that can be activated by certain stimuli.

With regard to the mapping of ISG15-targeting Lys site(s) within the AIF protein, we could not identify the exact site(s). There are several reports showing that ISGylation has relatively lower specificity to the substrate than other types of PTM, suggesting that adjacent lysine residues can be alternatively ISGylated (40, 42, 43). This much lower selectivity of ISG15 conjugation to the target is mainly due to the various innate immune responses required to protect cells from a large range of pathogens (44). Consistently, ISG15, unlike other ubiquitin modifiers, also has much lower specificity for the lysine residue of the target and is even more rarely conjugated to cysteine rather than lysine (32, 33, 39, 45). Presumably, this could be the reason why we were not able to map the exact ISGylation site(s) of tAIF. When all conserved lysine residues of tAIF were substituted with arginine individually or in various combinations, there was no significant difference of ISG15 conjugation between the WT and each mutant. Even if all of the available lysine groups of tAIF were replaced, ISGylated bands were still detected (Fig. S2), indicating that tAIF ISGylation does not occur at the conventional lysine residue site.

Based on the additional reports that cysteine can be modified by ISG15 (32, 33), we further examined whether cysteine residue(s) within the AIF could be a novel target of ISGylation. Contrary to expectations, it was observed that tAIF was still ISGylated even when both lysine and cysteine were mutated. Accordingly, these results indicated that ISGylation of tAIF may not target on Lys or Cys residues but on the novel site(s) that are not highly conserved, and these cases have been found in some of protein ubiquitination. Although ubiquitination mainly targets the lysine residues, numerous studies have reported the nonlysine-linked ubiquitination, occurring through nonamine groups, such as sulfhydryl groups of cysteine or hydroxyl groups of threonine and serine residues (46–50). Supporting to our data, there was a report suggesting that "noncanonical" conjugation of ISG15 to its target protein could also be possible (51). In this case, the target protein has no cysteine residue except for lysine residues, and all serine and threonine residues, which widely reported to be alternative conjugation sites in noncanonical ubiquitination studies, were substituted for the assay of ISG15-conjugation. Nevertheless, this mutant still showed to be ISGylated, suggesting that the complex regulatory mechanisms may underlie the ISGylation of target protein. The present study supports these hypotheses, and further studies would be required to expand the understanding of more complicated mechanism of protein ISGylation than can be expected.

We further found that ISG15 was induced by various stimuli, including IFN-α, etoposide, and camptothecin in A549 cells, and tAIF-ISGylation was also promoted by these stimuli. We also previously reported that, unlike the HEK293 cell line lacking some necessary components, ISGylation worked well in A549 cells (28). In addition, IFN-α treatment induced the ISGylation of the ubiquitin E3 ligase CHIP in the A549 cell line. Moreover, we have shown that ISG15 was significantly induced by DNA-damaging agents such as camptothecin and etoposide in various cell lines, including A549 cells (27). Accordingly, A549 cells were selected for this study. Moreover, numerous reports have shown that mitochondrial tAIF is released into the cytoplasm, inducing apoptosis in response to a variety of apoptosis-inducing agents, including staurosporine, etoposide, azide, tert-butylhydroperoxide, anisomycin, UV radiation, camptothecin, and MNNG (3, 52, 53). Since we observed that ISG15 and tAIF are mainly colocalized in the cytoplasm, we could assume that ISGylation of tAIF could be promoted by these apoptosis-inducing agents. Among the four apoptosis-inducing agents tested (*i.e.*, camptothecin, etoposide, MNNG, and staurosporine), ISG15 conjugation of AIF was significantly induced by camptothecin and etoposide in A549 cells. Although AIF is known to induce caspase-independent apoptosis by MNNG, ISG15 and subsequent tAIF-ISGylation were not induced by MNNG in A549 cells. Since etoposide and camptothecin are well-known caspase-dependent inducers of apoptosis, our results suggest that the downstream step(s) of cell death processes induced by ISGylated tAIF might involve caspase-dependent apoptotic events. Under this assumption, it would be interesting to further examine whether the signaling pathway of tAIF-ISGylation may accompany the release of cytochrome c followed by

caspase activation. Moreover, these results suggest that although apoptotic cell death induced by tAIF occurs in response to many toxic stimuli, their individual mechanisms and underlying regulatory modes could be different. Furthermore, the present results provide evidence that the specific conjugation of ISG15 to its targets (including AIF) largely depends on different cell types and stimuli (16, 27).

Truncated AIF is known to be ubiquitinated by CHIP and XIAP, differentially affecting the biochemical and physical properties of tAIF (10, 11). For example, CHIP destabilizes and eventually degrades tAIF *via* proteasome-dependent ubiquitination, resulting in the inhibition of apoptosis. XIAP inhibits apoptosis by ubiquitination of AIF at K255, enhancing its binding to DNA and chromatin degradation. Similar to the latter case, we have previously shown that ISGylation affects the ubiquitination of Parkin and CHIP, positively affecting Parkin and CHIP activities (27, 28). In line with these previous studies, in this study, we first tested whether ISGylation affects the ubiquitination of tAIF. Consequently, we found that ISGylation increased the ubiquitination of tAIF, which occurs through a nonclassical K6 ubiquitin linkage mechanism. Accumulating evidence suggests that K6 ubiquitin linkage may be involved in protein stabilization (54–56) and other non-degradative regulation of targets, including mitophagic protein regulation (57–59). Recently, another novel function of K6-linked ubiquitination was revealed: it enhances the DNA-binding capacity of the substrate in the innate immune system response (60). More precisely, the transcription factor IRF3 is ubiquitinated *via* K6-linkage upon viral infection, causing IRF3 to interact with the promoter of type I IFN genes and ultimately enhancing antiviral innate immunity. Considering the multiple functions of K6-linked ubiquitination in the preceding cases, it can be inferred that the K6-linked ubiquitination of ISGylated tAIF is also likely to contribute to the stabilization of tAIF, as well as its nuclear translocation and DNA-binding capacity.

We further investigated whether the stability of tAIF was affected by ISGylation. Our results indicated that ISGylation increases the half-life of tAIF. We found that the half-life of ectopic tAIF was significantly reduced when *HERC5* expression was knocked down (Fig. 5*B*). In addition, we investigated whether the de-ISGylating enzyme UBP43 could also negatively affect the half-life of ectopic tAIF (Fig. 5*D*). The half-life of ectopic tAIF was also reduced when it was measured in the presence of conjugation-deficient ISG15-AA as a dominant-negative mutant (Fig. 5*F*). In addition, the half-life of endogenous tAIF was significantly reduced by *HERC5*-knockdown and etoposide treatment (Fig. 5*G*). In contrast to the effect of the CHIP-mediated ubiquitination of tAIF to suppress neuronal cell death through the degradation of tAIF, we speculated that apoptosis would be enhanced by ISGylation through the stabilization of tAIF.

Next, we examined whether ISGylation also affects the nuclear translocation of tAIF. Cell fractionation and immunofluorescence analyses and the PLA verified that treatment with etoposide or camptothecin increased the ISGylation of AIF itself in all fractions, in particular promoting the nuclear translocation of tAIF simultaneously. This finding was further confirmed when the expression of *AIF* and *HERC5* was knocked down in A549 cells, resulting in proportional suppression of apoptotic cell death. These results support our hypothesis that the ISGylation of tAIF causes the K6-linked ubiquitination and stabilization of tAIF, eventually promoting cell death. Since AIF and its homologs are ubiquitously present in several tissues and cells other than the lung and A549 cells and defective PTMs, including ISGylation, are closely linked with many human diseases, a complete understanding of tAIF-ISGylation would be critical for future therapeutic development and treatment of diverse AIF-related diseases.

Taken together, the present finding of an additional PTM mode (*i.e.*, ISGylation) for the regulation of apoptotic tAIF activity indirectly highlights the functional importance of AIF within cells, for example, in the maintenance of cellular homeostasis. In addition, our data support the hypothesis that the induction of ISG15 and subsequent ISGylation of protein target(s) has a novel regulatory role that contributes to toxic stimuli-induced cell death.

Experimental procedures

Materials

Dulbecco's modified Eagle's medium (DMEM) and fetal bovine serum were purchased from Corning Life Science. Lipofectamine 2000 and Ni-NTA agarose beads were purchased from Invitrogen. Protein A-Sepharose beads were purchased from GE Healthcare Life Sciences. Protein G-agarose 4B resin was purchased from Lugen Sci. Enhanced chemiluminescence reagents were purchased from PerkinElmer Life and Analytical Sciences, AbClon, and Advansta. IFN-α was purchased from PBL Assay Science. MG132 was purchased from AG Scientific. Camptothecin (C9911), etoposide (E1383), staurosporine (S4400), and cycloheximide (C4859) were purchased from Sigma–Aldrich. MNNG (M0527) was purchased from Tokyo Chemical Industry. The monoclonal anti-V5 antibody (46-0705) was purchased from Invitrogen. Monoclonal anti-FLAG (F3165) antibodies were purchased form Sigma–Aldrich. Monoclonal anti-AIF (sc-13116), monoclonal anti-HSP90 (sc-13119), monoclonal anti-β-actin (sc-47778), monoclonal anti-ISG15 (sc-166755), polyclonal anti-ISG15 (H150; sc-50366), monoclonal anti-Myc (sc-40), monoclonal antiubiquitin (sc-8017), and polyclonal anti-HDAC3 (sc-11417) antibodies were purchased from Santa Cruz Biotechnology. Polyclonal anti-AIF (4642S) and polyclonal anti-VDAC1 (4866) antibodies were purchased form Cell Signaling Technology. Monoclonal anti-hemagglutinin (HA) antibody (MMS-101P) was purchased from Covance. Polyclonal mouse anti-HERC5 (H00051191-A01) was obtained from Novus Biologicals. Monoclonal antitubulin (GTX628802) was purchased from Genetex. Polyclonal antihistone H3 (ab1191) and polyclonal anti-V5 (ab9116) antibodies were purchased from Abcam. Mouse IgG (12-371), rabbit IgG (12-

370), peroxidase-conjugated mouse IgG (AP124P), and peroxidase-conjugated rabbit IgG (AP132P) were purchased from Millipore. Alexa Fluor 488–conjugated antimouse (A-11029) and Alexa Fluor 594–conjugated anti-rabbit (A-11012) secondary antibodies were purchased from Invitrogen.

DNA constructs

Plasmids encoding V5-His-tagged rat full-length AIF and its truncated form lacking the N-terminal 101 amino acids (pcDNA4.1-V5-His/TOPO-AIF and pcDNA4.1-V5-His/TOPO-tAIF), FLAG-tagged WT ISG15 (pFLAG-ISG15-WT) and its conjugation-defective mutant (pFLAG-ISG15-AA), WT UBE1L (pcDNA-UBE1L), Myc-tagged UbcH8, and Myc-tagged EFP were kindly provided by C.H. Chung (Seoul National University, Seoul, Korea). Mammalian construct encoding HA-tagged UbcH8 (pRK5-HA-UbcH8) was a kind gift from T. M. Dawson (Johns Hopkins University School of Medicine, Baltimore, MD, USA). The plasmid encoding FLAG-tagged HERC5 was kindly provided by K. Hochrainer (Weill Cornell Medical College, New York, NY, USA). The plasmid encoding FLAG-tagged HHARI (pFLAG-HHARI) was kindly provided by D. E. Zhang (University of California at San Diego, San Diego, CA, USA). Several plasmids encoding either WT tAIF with V5-His-tagging at the C terminus (tAIF-V5-His) or its point mutants having a substitution of lysine with arginine at the indicated single or multiple sites were produced by site-directed mutagenesis using the QuikChange XL Site-directed Mutagenesis kit (Stratagene). All DNA sequences were confirmed by sequencing (BIONICS).

Cell culture and DNA transfection

HEK293 cells and human lung carcinoma A549 cells were maintained in DMEM supplemented with 10% fetal bovine serum and 100 U/ml penicillin–streptomycin. The cells were grown at 37 °C in a humidified atmosphere containing 5% CO_2. All DNA transfections were performed using Lipofectamine 2000 according to the manufacturer's protocol. To induce apoptotic cell death, the cells were treated with 50 or 100 μM etoposide for 36 or 24 h, respectively.

RNAi

siRNAs targeting *HERC5*, *AIF* (catalog no.: # 9131-2), or *ISG15* (catalog no.: #9636-1) were synthesized by Bioneer. Scrambled siRNA (catalog no.: # 51-01-14-04) as a negative control was purchased from Integrated DNA Technologies. The *HERC5*-specific siRNA duplex sense and antisense sequences were 5′-GGACUAGACAAUCAGAAAGdTdT-3′ and 5′- CUUUCUGAUUGUCUAGUCC dTdT-3′, respectively.

Immunoprecipitation and Western blotting analysis

Cultured cells were harvested by scraping with ice-cold PBS and washed with PBS. Cells were then incubated at 4 °C for 30 min with radioimmunoprecipitation assay buffer containing 50 mM Tris (pH 7.5), 150 mM NaCl, 1% Triton X-100, 0.5% sodium deoxycholate, and 0.1% SDS. Aliquots of protease inhibitor cocktail including 0.2 mM PMSF, 1 μg/ml aprotinin, 1 μg/ml leupeptin, 1 mM Na_3VO_4, and 10 mM NaF were added to the cell lysates just before use. Cell lysates were then vortexed every 10 min, centrifuged at 15,000×*g* for 15 min at 4 °C, and the supernatants were collected into clean tubes. For immunoprecipitation, cell lysates including 0.5 to 2 mg of protein were incubated with the appropriate antibody overnight at 4 °C with gentle rotation. The samples were incubated with either Protein A-Sepharose or Protein G-Agarose beads, incubated for 2 h at 4 °C, centrifuged at 9300×*g* for 30 s, and washed three times with radioimmunoprecipitation assay lysis buffer. Immunocomplexes were collected by centrifugation at 8000×*g* for 1 min, and bead-bound proteins were eluted by adding 2× SDS-PAGE sample buffer. The samples were denatured by boiling for 5 min, separated on SDS-PAGE gels, and transferred onto nitrocellulose membranes. Membranes were blocked for 1 h at room temperature (RT) in 1× TBST buffer (25 mM Tris [pH 7.6], 137 mM NaCl and 0.1% Tween 20) containing 5% nonfat dry milk and incubated with the appropriate primary antibody overnight at 4 °C. The membranes were then washed with TBST, incubated for 2 h with horseradish peroxidase–conjugated secondary IgG, washed again with TBST, and visualized using enhanced chemiluminescence reagents following the manufacturer's instructions.

Ni-NTA pull-down analysis

Cells were harvested by scraping with ice-cold PBS, washed with PBS, and lysed for 30 min at RT in lysis buffer containing 0.1 M NaH_2PO_4/Na_2HPO_4 (pH 7.4), 8 M urea, 10 mM imidazole, and a protease inhibitor cocktail. Cell lysates were vortexed every 10 min, centrifuged at 15,000×*g* for 20 min at RT, and the supernatants were collected into clean tubes. The samples were then incubated with Ni-NTA agarose beads for 90 min at RT, washed three times with lysis buffer containing 50 mM imidazole, and the bound proteins were then eluted with the same buffer containing 500 mM imidazole. The samples were incubated in SDS sample buffer for 5 min at RT and separated by SDS-PAGE.

Subcellular protein fractionation assay

After A549 cells were harvested by scraping with ice-cold PBS, subcellular fractionation was performed using a subcellular protein fractionation kit (catalog no.: #78840, Thermo Fisher Scientific) according to the manufacturer's protocol. Protein extracts from the cytoplasm, membrane fractions, soluble nucleus, and chromatin-bound nucleus were sequentially obtained.

Immunocytochemistry analysis

A549 cells were cultured on poly-L-lysine–coated glass coverslips in 6-well plates. The cells were treated with either etoposide or camptothecin, harvested, washed twice with PBS buffer, and fixed in 3.7% formaldehyde for 10 min at RT. Cells were then permeabilized with 0.2% Triton X-100 for 10 min, blocked with 1% bovine serum albumin in PBS for 1 h at RT, and stained with anti-ISG15 or anti-AIF antibodies for 16 h at 4 °C. The samples were incubated with Alexa Fluor 488–

conjugated antimouse or Alexa Fluor 594–conjugated anti-rabbit secondary antibodies to detect the primary antibodies. Images were captured using an LSM 880 laser scanning confocal microscope (Carl Zeiss) and the data were processed using Zeiss LSM Image Browser (Carl Zeiss). To quantify the colocalization of ISG15 and AIF proteins within cells, Image J software (National Institutes of Health) was used to calculate Pearson's correlation coefficient.

PLA

A PLA was performed using the Duolink PLA assay kit (DUO92101, Sigma–Aldrich), following the manufacturer's protocols. The PLA signals are displayed in red and the nuclei are shown in blue. To quantify the PLA signals, Image J software was used for analysis.

LDH cytotoxicity assay

Cellular cytotoxicity was measured using an LDH cytotoxicity assay kit (MK401; Takara), according to the manufacturer's instructions. Briefly, after DNA or siRNA transfection for 48 h, A549 cells were left untreated or treated with 100 μM etoposide for an additional 24 h. Cell-free culture media were then transferred to sterile 96-well plates, and the appropriate mixture of solutions was added to each well. The plates were incubated for up to 30 min at RT to determine the LDH activity in the supernatant. The absorbance of each sample was measured at 490 to 492 nm using a microplate reader.

Flow cytometry analysis of apoptotic cells

Apoptosis of A549 cells was analyzed by using Annexin V-FITC Apoptosis Staining/Detection Kit (ab14085, Abcam), according to the supplier's instructions. Cells were cultured in 6-well plates, harvested, and stained with Annexin V-FITC and/or PI for analysis with a BD FACS LSR II SORP system (Becton Dickinson).

Statistical analysis

One-way ANOVA with unpaired *t* tests was used for all statistical analyses to compare data from different groups. The analysis was performed using SPSS statistical analysis software (version 25.0; IBM). All values are reported as mean ± SEM; *p* values less than 0.05 were considered statistically significant, and the sample size for each experiment (n) is noted in the corresponding figure legends. The intensities of the Western blot bands were measured using GelQuant.NET software (version 1.8.2; biochemlabsolutions.com).

Data availability

All datasets are included within the article or are available from the corresponding author: Kwang Chul Chung (kchung@yonsei.ac.kr).

Supporting information—This article contains supporting information.

Acknowledgments—We thank C. H. Chung, T. M. Dawson, K. Hochrainer, and D. E. Zhang for providing various plasmids; H. S. Cho for performing the structural analysis of AIF; and L. Yoo for helpful discussions and comments.

Author contributions—K. C. C. conceptualization; S. J. J. methodology; S. J. J. validation; S. J. J. and K. C. C. formal analysis; S. J. J. and K. C. C. investigation; S. J. J. data curation; S. J. J. and K. C. C. writing–original draft; S. J. J. and K. C. C. writing–review & editing.

Funding and additional information—This work was supported by a National Research Foundation of Korea (NRF) grant funded by the Ministry of Science and ICT, Korea government (NRF-2021R1A2C1005469 to K. C. C.).

Conflict of interest—The authors declare that they have no conflicts of interest with the contents of this article.

Abbreviations—The abbreviations used are: AIF, apoptosis-inducing factor; co-IP, coimmunoprecipitation; HA, hemagglutinin; HEK293, human embryonic kidney 293; LDH, lactate dehydrogenase; MNNG, N-methyl-N-nitro-N′-nitrosoguanidine; PI, propidium iodide; PLA, proximity ligation assay; PTM, posttranslational modification; tAIF, truncated AIF.

References

1. Lorenzo, H. K., Susin, S. A., Penninger, J., and Kroemer, G. (1999) Apoptosis inducing factor (AIF): a phylogenetically old, caspase-independent effector of cell death. *Cell Death Differ.* **6**, 516–524
2. Daugas, E., Nochy, D., Ravagnan, L., Loeffler, M., Susin, S. A., Zamzami, N., *et al.* (2000) Apoptosis-inducing factor (AIF): a ubiquitous mitochondrial oxidoreductase involved in apoptosis. *FEBS Lett.* **476**, 118–123
3. Sevrioukova, I. F. (2011) Apoptosis-inducing factor: structure, function, and redox regulation. *Antioxid. Redox Signal* **14**, 2545–2579
4. Natarajan, S. K., and Becker, D. F. (2012) Role of apoptosis-inducing factor, proline dehydrogenase, and NADPH oxidase in apoptosis and oxidative stress. *Cell Health Cytoskelet* **2012**, 11–27
5. Liu, L., Xing, D., and Chen, W. R. (2009) Micro-calpain regulates caspase-dependent and apoptosis inducing factor-mediated caspase-independent apoptotic pathways in cisplatin-induced apoptosis. *Int. J. Cancer* **125**, 2757–2766
6. Polster, B. M., Basañez, G., Etxebarria, A., Hardwick, J. M., and Nicholls, D. G. (2005) Calpain I induces cleavage and release of apoptosis-inducing factor from isolated mitochondria. *J. Biol. Chem.* **280**, 6447–6454
7. Yu, S.-W., Wang, H., Poitras, M. F., Coombs, C., Bowers, W. J., Federoff, H. J., *et al.* (2002) Mediation of poly(ADP-ribose) polymerase-1-dependent cell death by apoptosis-inducing factor. *Science* **297**, 259–263
8. Xing, Y., Li, Y., Hu, B., Han, F., Zhao, X., Zhang, H., *et al.* (2021) PAK5-mediated AIF phosphorylation inhibits its nuclear translocation and promotes breast cancer tumorigenesis. *Int. J. Biol. Sci.* **17**, 1315–1327
9. Wesierska-Gadek, J., Gueorguieva, M., Schloffer, D., Uhl, M., and Wojciechowski, J. (2003) Non-apoptogenic killing of hela cervical carcinoma cells after short exposure to the alkylating agent N-methyl-N'-nitro-N-nitrosoguanidine (MNNG). *J. Cell Biochem.* **89**, 1222–1234
10. Oh, K., Yang, S., Park, J., Seol, J. H., Iemura, S., Natsume, T., *et al.* (2011) Control of AIF-mediated cell death by antagonistic functions of CHIP ubiquitin E3 ligase and USP2 deubiquitinating enzyme. *Cell Death Differ.* **18**, 1326–1336
11. Wilkinson, J. C., Wilkinson, A. S., Galbán, S., Csomos, R. A., and Duckett, C. S. (2008) Apoptosis-inducing factor is a target for ubiquitination through interaction with XIAP. *Mol. Cell Biol.* **28**, 237–247
12. Lewis, E. M., Wilkinson, A. S., Davis, N. Y., Horita, D. A., and Wilkinson, J. C. (2011) Nondegradative ubiquitination of apoptosis inducing factor (AIF) by X-linked inhibitor of apoptosis at a residue critical for AIF-mediated chromatin degradation. *Biochemistry* **50**, 11084–11096

13. Haas, A. L., Ahrens, P., Bright, P. M., and Ankel, H. (1987) Interferon induces a 15-kilodalton protein exhibiting marked homology to ubiquitin. *J. Biol. Chem.* **262**, 11315–11323
14. Loeb, K. R., and Haas, A. L. (1992) The interferon-inducible 15-kDa ubiquitin homolog conjugates to intracellular proteins. *J. Biol. Chem.* **267**, 7806–7813
15. Ritchie, K. J., and Zhang, D. E. (2004) ISG15: the immunological kin of ubiquitin. *Semin. Cell Dev. Biol.* **15**, 237–246
16. Zhang, D., and Zhang, D. E. (2011) Interferon-stimulated gene 15 and the protein ISGylation system. *J. Interferon Cytokine Res.* **31**, 119–130
17. Malakhov, M. P., Malakhova, O. A., Kim, K. I., Ritchie, K. J., and Zhang, D. E. (2002) UBP43 (USP18) specifically removes ISG15 from conjugated proteins. *J. Biol. Chem.* **277**, 9976–9981
18. Dzimianski, J. V., Scholte, F. E. M., Bergeron, É., and Pegan, S. D. (2019) ISG15: it's complicated. *J. Mol. Biol.* **431**, 4203–4216
19. Jeon, Y. J., Choi, J. S., Lee, J. Y., Yu, K. R., Kim, S. M., Ka, S. H., *et al.* (2009) ISG15 modification of filamin B negatively regulates the type I interferon-induced JNK signalling pathway. *EMBO Rep.* **10**, 374–380
20. Zou, W., Papov, V., Malakhova, O., Kim, K. I., Dao, C., Li, J., *et al.* (2005) ISG15 modification of ubiquitin E2 Ubc13 disrupts its ability to form thioester bond with ubiquitin. *Biochem. Biophys. Res. Commun.* **336**, 61–68
21. Shi, H. X., Yang, K., Liu, X., Liu, X. Y., Wei, B., Shan, Y. F., *et al.* (2010) Positive regulation of interferon regulatory factor 3 activation by Herc5 via ISG15 modification. *Mol. Cell Biol.* **30**, 2424–2436
22. D'Cunha, J., Ramanuiam, S., Wagner, R. J., Witt, P. L., Knight, E., Jr., and Borden, E. C. (1996) *In vitro* and *in vivo* secretion of human ISG15, an IFN-induced immunomodulatory cytokine. *J. Immunol.* **157**, 4100–4108
23. D'Cunha, J., Knight, E., Jr., Haas, A. L., Truitt, R. L., and Border, E. C. (1996) Immunoregulatory properties of ISG15, an interferon-induced cytokine. *Proc. Natl. Acad. Sci. U.S.A.* **93**, 211–215
24. Giannakopoulos, N. V., Luo, J. K., Papov, V., Zou, W., Lenschow, D. J., Jacobs, B. S., *et al.* (2005) Proteomic identification of proteins conjugated to ISG15 in mouse and human cells. *Biochem. Biophys. Res. Commun.* **336**, 496–506
25. Zhao, C., Denison, C., Huibregtse, J. M., Gygi, S., and Krug, R. M. (2005) Human ISG15 conjugation targets both IFN-induced and constitutively expressed proteins functioning in diverse cellular pathways. *Proc. Natl. Acad. Sci. U.S.A.* **102**, 10200–10205
26. Takeuchi, T., Inoue, S., and Yokosawa, H. (2006) Identification and Herc5-mediated ISGylation of novel target proteins. *Biochem. Biophys. Res. Commun.* **348**, 473–477
27. Im, E., Yoo, L., Hyun, M., Shin, W. H., and Chung, K. C. (2016) Covalent ISG15 conjugation positively regulates the ubiquitin E3 ligase activity of parkin. *Open Biol.* **6**, 160193
28. Yoo, L., Yoon, A. R., Yun, C. O., and Chung, K. C. (2018) Covalent ISG15 conjugation to CHIP promotes its ubiquitin E3 ligase activity and inhibits lung cancer cell growth in response to type I interferon. *Cell Death Dis.* **9**, 97
29. Albert, M., Bécares, M., Falqui, M., Fernández-Lozano, C., and Guerra, S. (2018) ISG15, a small molecule with huge implications: regulation of mitochondrial homeostasis. *Viruses* **10**, 629
30. Okumura, F., Okumura, A. J., Uematsu, K., Hatakeyama, S., Zhang, D. E., and Kamura, T. (2013) Activation of double-stranded RNA-activated protein kinase (PKR) by interferon-stimulated gene 15 (ISG15) modification down-regulates protein translation. *J. Biol. Chem.* **288**, 2839–2847
31. Oh, Y., and Chung, K. C. (2012) Small ubiquitin-like modifier (SUMO) modification of zinc finger protein 131 potentiates its negative effect on estrogen signaling. *J. Biol. Chem.* **287**, 17517–17529
32. Bade, V. N., Nickels, J., Keusekotten, K., and Praefcke, G. J. (2012) Covalent protein modification with ISG15 via a conserved cysteine in the hinge region. *PLoS One* **7**, e38294
33. Huang, Y. F., Wee, S., Gunaratne, J., Lane, D. P., and Bulavin, D. V. (2014) Isg15 controls p53 stability and functions. *Cell Cycle* **13**, 2200–2210
34. Liu, M., Hummer, B. T., Li, X., and Hassel, B. A. (2004) Camptothecin induces the ubiquitin-like protein, ISG15, and enhances ISG15 conjugation in response to interferon. *J. Interferon Cytokine Res.* **24**, 647–654
35. Zhang, X. D., Gillespie, S. K., and Hersey, P. (2004) Staurosporine induces apoptosis of melanoma by both caspase-dependent and -independent apoptotic pathways. *Mol. Cancer Ther.* **3**, 187–197
36. Abe, T., Minami, N., Bawono, R. G., Matsui, C., Deng, L., Fukuhara, T., *et al.* (2020) ISGylation of hepatitis C virus NS5A protein promotes viral RNA replication via recruitment of cyclophilin A. *J. Virol.* **94**, e00532-20
37. Takeuchi, T., and Yokosawa, H. (2008) Detection and analysis of protein ISGylation. *Methods Mol. Biol.* **446**, 139–149
38. Zhao, C., Hsiang, T. Y., Kuo, R. L., and Krug, R. M. (2010) ISG15 conjugation system targets the viral NS1 protein in influenza A virus-infected cells. *Proc. Natl. Acad. Sci. U.S.A.* **107**, 2253–2258
39. Vuillier, F., Li, Z., Commere, P. H., Dynesen, L. T., and Pellegrini, S. (2019) USP18 and ISG15 coordinately impact on SKP2 and cell cycle progression. *Sci. Rep.* **9**, 4066
40. Park, J. M., Yang, S. W., Yu, K. R., Ka, S. H., Lee, S. W., Seol, J. H., *et al.* (2014) Modification of PCNA by ISG15 plays a crucial role in termination of error-prone translesion DNA synthesis. *Mol. Cell* **54**, 626–638
41. Oh, Y., and Chung, K. C. (2013) UHRF2, a ubiquitin E3 ligase, acts as a small ubiquitin-like modifier E3 ligase for zinc finger protein 131. *J. Biol. Chem.* **288**, 9102–9111
42. Xu, D., Zhang, T., Xiao, J., Zhu, K., Wei, R., Wu, Z., *et al.* (2015) Modification of BECN1 by ISG15 plays a crucial role in autophagy regulation by type I IFN/interferon. *Autophagy* **11**, 617–628
43. Jin, J., Meng, X., Huo, Y., and Deng, H. (2021) Induced TRIM21 ISGylation by IFN-β enhances p62 ubiquitination to prevent its autophagosome targeting. *Cell Death Dis.* **12**, 697
44. Durfee, L. A., Lyon, N., Seo, K., and Huibregtse, J. M. (2010) The ISG15 conjugation system broadly targets newly synthesized proteins: implications for the antiviral function of ISG15. *Mol. Cell* **38**, 722–732
45. Okumura, F., Zou, W., and Zhang, D. E. (2007) ISG15 modification of the eIF4E cognate 4EHP enhances cap structure-binding activity of 4EHP. *Genes Dev.* **21**, 255–260
46. Vosper, J. M., McDowell, G. S., Hindley, C. J., Fiore-Heriche, C. S., Kucerova, R., Horan, I., *et al.* (2009) Ubiquitylation on canonical and non-canonical sites targets the transcription factor neurogenin for ubiquitin-mediated proteolysis. *J. Biol. Chem.* **284**, 15458–15468
47. Tatham, M. H., Plechanovová, A., Jaffray, E. G., Salmen, H., and Hay, R. T. (2013) Ube2W conjugates ubiquitin to α-amino groups of protein N-termini. *Biochem. J.* **453**, 137–145
48. Wang, X., Herr, R. A., Chua, W. J., Lybarger, L., Wiertz, E. J., and Hansen, T. H. (2007) Ubiquitination of serine, threonine, or lysine residues on the cytoplasmic tail can induce ERAD of MHC-I by viral E3 ligase mK3. *J. Cell Biol.* **177**, 613–624
49. Cadwell, K., and Coscoy, L. (2005) Ubiquitination on nonlysine residues by a viral E3 ubiquitin ligase. *Science* **309**, 127–130
50. McClellan, A. J., Laugesen, S. H., and Ellgaard, L. (2019) Cellular functions and molecular mechanisms of non-lysine ubiquitination. *Open Biol.* **9**, 190147
51. Park, S. Y., Yoon, S., Kim, H., and Kim, K. K. (2016) 90K Glycoprotein promotes degradation of mutant β-catenin lacking the ISGylation or phosphorylation sites in the N-terminus. *Neoplasia* **18**, 618–625
52. Cregan, S. P., Fortin, A., MacLaurin, J. G., Cecconi, F., Yu, S. W., Dawson, T. M., *et al.* (2002) Apoptosis-inducing factor is involved in the regulation of caspase-independent neuronal cell death. *J. Cell Biol.* **158**, 507–517
53. Lee, M. W., Kim, W. J., Beardsley, D. I., and Brown, K. D. (2007) N-methyl-N'-nitro-N-nitrosoguanidine activates multiple cell death mechanisms in human fibroblasts. *DNA Cell Biol.* **26**, 683–694
54. Srivastava, D., and Chakrabarti, O. (2014) Mahogunin-mediated α-tubulin ubiquitination via noncanonical K6 linkage regulates microtubule stability and mitotic spindle orientation. *Cell Death Dis.* **5**, e1064
55. Mukherjee, R., Majumder, P., and Chakrabarti, O. (2017) MGRN1-mediated ubiquitination of α-tubulin regulates microtubule dynamics and intracellular transport. *Traffic* **18**, 791–807
56. Tracz, M., and Bialek, W. (2021) Beyond K48 and K63: non-canonical protein ubiquitination. *Cell Mol. Biol. Lett.* **26**, 1
57. Ordureau, A., Heo, J., Duda, D. M., Paulo, J. A., Olszewski, J. L., and Yanishevski, D. (2015) Defining roles of PARKIN and ubiquitin

phosphorylation by PINK1 in mitochondrial quality control using a ubiquitin replacement strategy. *Proc. Natl. Acad. Sci. U.S.A.* **112**, 6637–6642

58. Durcan, T. M., Tang, M. Y., Pérusse, J. R., Dashti, E. A., Aguileta, M. A., Mclelland, L., *et al.* (2014) USP8 regulates mitophagy by removing K6 -linked ubiquitin conjugates from parkin. *EMBO J.* **33**, 2473–2491
59. Cunningham, C. N., Baughman, J. M., Phu, L., Tea, J. S., Yu, C., Coons, M., *et al.* (2015) USP30 and parkin homeostatically regulate atypical ubiquitin chains on mitochondria. *Nat. Cell Biol.* **17**, 160–169
60. Zhang, Z., Wang, D., Wang, P., Zhao, Y., and You, F. (2020) OTUD1 negatively regulates type i IFN induction by disrupting noncanonical ubiquitination of IRF3. *J. Immunol.* **204**, 1904–1918